PHYSICS WITH LOW-ENERGY MUONS AT A NEUTRINO FACTORY COMPLEX

J. Äystö[1], *A. Baldini*[2], *A. Blondel*[3], *A. de Gouvêa*[4], *J. Ellis*[4], *W. Fetscher*[5], *G.F. Giudice*[4], *K. Jungmann*[6], *S. Lola*[4], *V. Palladino*[7], *K. Tobe*[4], *A. Vacchi*[8], *A. van der Schaaf*[9], *K. Zuber*[10]
[1]Jyvaskyla University, Finland.
[2]INFN Pisa, Italy.
[3]Geneva University, Switzerland.
[4]CERN, Geneva, Switzerland.
[5]ETH, Zürich, Switzerland.
[6]KVI, Groningen, The Netherlands.
[7]Università Federico II and INFN Napoli, Italy.
[8]INFN Trieste, Italy.
[9]Physik-Institut der Universität Zürich, Switzerland.
[10]Dortmund University, Germany.

Abstract

The physics potential of an intense source of low-energy muons is studied. Such a source is a necessary stage towards building the neutrino factories and muon colliders which are being considered at present. The CERN Neutrino Factory could deliver muon beams with intensities 3–4 orders of magnitude higher than available now, with large freedom in the choice of the time structure. Low-energy muon physics contributes to many fields of basic research, including rare muon decays, i.e., decays that do not conserve muon number, measurements of fundamental constants, the muon anomalous magnetic moment, determination of the Lorentz structure of the weak interaction, QED tests, CPT tests, proton and nuclear charge distributions (even for short-lived isotopes), and condensed matter physics. In studying the experimental programme, we analyse the present limitations, list the requirements on the new muon beams, and describe some ideas on how to implement these beam lines in a CERN neutrino factory complex.

CERN-TH/2001–231

Contents

1 INTRODUCTION

Ever since the discovery of the muon the study of its properties has contributed to a deeper understanding of Nature at the smallest distance scale. Muon physics played a fundamental role in establishing the V–A structure of weak interactions and the validity of quantum electrodynamics. Moreover, muon physics has not yet exhausted its potential and, indeed, may provide crucial information regarding one of the most fundamental quests in modern physics: the structure of the theory which lies beyond the Standard Model of particle physics.

Muon storage rings are currently, and seriously, being considered as options for future endeavors of accelerator laboratories such as CERN and Fermilab. The primary aim of the machine presently considered is the study of neutrino properties, hence they are also referred to as neutrino factories (NUFACT). They are a first step towards a still more ambitious goal: muon colliders, capable of 'precision' Higgs physics and the exploration of the highest energy frontier.

Neutrino factories are also an ideal place to study muon properties, since they provide, necessarily, muon fluxes which are orders of magnitude larger than what can be obtained at present. It is, therefore, imperative to understand how to take full advantage of these intense muon beams in order to significantly improve on the reach of stopped-muon experiments. This is the aim of this part of the report.

While precise measurements of the muon lifetime and Michel parameters provide tests for the theory of weak interactions and its possible extensions, one of the main interests in muon physics lies in the search for processes that violate muon number. The discovery of decays such as $\mu^+ \to e^+\gamma$ and $\mu^+ \to e^+e^-e^+$ or of μ^-–e^- conversion in nuclei would be an indisputable proof of the existence of new dynamics beyond the Standard Model.

Global symmetries (like individual lepton numbers), as opposed to local symmetries, are considered not to be based on fundamental principles and are expected to be violated by gravitational effects, in the strong regime, and, more generally, by higher-dimensional effective operators which describe local interactions originating from some unknown high-energy dynamics. Baryon number conservation is another example of an Abelian global symmetry of the Standard Model, which can be broken by new-physics effects.

Atmospheric and solar neutrino experiments have provided strong evidence for neutrino oscillations. This implies violation of individual lepton numbers (L_i) and, most likely, of total lepton number (L), which is a first indication of physics beyond the Standard Model. Current neutrino data indicate values of the neutrino masses corresponding to non-renormalizable interactions at a scale $M \sim 10^{9-14}$ GeV. New lepton-number violating dynamics at the scale M cannot yield observable rates for rare muon processes, since the corresponding effects are suppressed by $(m_\mu/M)^4$. The observation of muon-number violation in muon decays would thus require new physics beyond the one responsible for neutrino masses. Theoretically, however, there is no reason why L_i and L would be broken at the same energy scale. Indeed, in many frameworks, such as supersymmetry, the L_i breaking scale can be close to the weak scale. In this case, muon processes with L_μ violation would occur with rates close to the current experimental bounds.

It is also very important to stress that the information which can be extracted from the study of rare muon processes is, in many cases, not accessible to high-energy colliders. Take supersymmetry as an example. While the LHC can significantly probe slepton masses, it cannot compete with muon-decay experiments in constraining the slepton mixing angles.

In Section 2 we discuss 'normal' muon decay and its importance to fundamental physics. In Section 3 we address muon-number violating processes, first discussing the theoretical expectations and then addressing the issue of how to improve on current experimental bounds given a larger muon flux. In particular we discuss which elements of the experimental set-ups need to be improved or drastically modified. In Section 4 we address the measurements of fundamental properties of the muon, and in Section 5 we discuss bound muon systems (muonic atoms and condensed matter systems). In Section 6

we summarize the beam requirements imposed by the various experiments and discuss how these could be met in a neutrino factory complex. Our conclusions are given in Section 7.

2 NORMAL MUON DECAY

2.1 Theoretical background

All measurements in normal muon decay, $\mu^- \to e^- \overline{\nu}_e \nu_\mu$, and its inverse, $\nu_\mu e^- \to \mu^- \nu_e$, are successfully described by the 'V–A' interaction, which is a particular case of the local, derivative-free, lepton-number-conserving, four-fermion interaction [1]. The 'V–A' form and the nature of the neutrinos ($\overline{\nu}_e$ and ν_e) have been determined by experiment [2, 3].

The observables in muon decay (energy spectra, polarizations and angular distributions) and in inverse muon decay (the reaction cross section) at energies well below $m_W c^2$ may be parametrized in terms of the dimensionless coupling constants $g^\gamma_{\varepsilon\mu}$ and the Fermi coupling constant G_F. The matrix element is

$$\mathcal{M} = \frac{4G_\mathrm{F}}{\sqrt{2}} \sum_{\substack{\gamma=\mathrm{S,V,T} \\ \varepsilon,\mu=\mathrm{R,L}}} g^\gamma_{\varepsilon\mu} \langle \overline{e}_\varepsilon | \Gamma^\gamma | (\nu_e)_n \rangle \langle (\overline{\nu}_\mu)_m | \Gamma_\gamma | \mu_\mu \rangle \ . \tag{1}$$

We use here the notation of Fetscher *et al.*, [2, 4] who in turn use the sign conventions and definitions of Scheck [5]. Here $\gamma = \mathrm{S, V, T}$ indicate a (Lorentz) scalar, vector, or tensor interaction, and the chirality of the electron or muon (right- or left-handed) is labelled by $\varepsilon, \mu = \mathrm{R, L}$. The chiralities n and m of the ν_e and the $\overline{\nu}_\mu$ are determined by given values of γ, ε and μ. The 10 complex amplitudes $g^\gamma_{\varepsilon\mu}$ and G_F constitute 19 independent parameters to be determined by experiment. The 'V–A' interaction corresponds to $g^\mathrm{V}_\mathrm{LL} = 1$, with all other amplitudes being 0.

With the deduction *from experiments* that the interaction is predominantly of the vector type and left-handed [$g^\mathrm{V}_\mathrm{LL} > 0.96$ (90 %CL)], there remain several separate routes of investigation of normal muon decay, which will be discussed in the following.

2.2 Muon lifetime measurements

The measurement of the muon lifetime yields the most precise determination of the Fermi coupling constant G_F, which is presently known with a relative precision of 9×10^{-6}. Improving this measurement is certainly an interesting goal [6], since G_F is one of the fundamental parameters of the Standard Model. A clean beam pulse structure with very good suppression of particles between pulses is indispensable. Presently three experiments are in progress, two of which are at PSI [7] and one is located at RAL [8]. An improvement in the precision of τ_μ by about a factor of 20 can be expected. An additional order of magnitude could be gained at a neutrino factory primarily from increased muon flux with the major systematics being pile-up and detector timing stability.

There are two caveats, however:

- Reducing the error on G_F by precise measurements of the muon lifetime would unfortunately not improve the electroweak fits, because the error on the dimensionless input $G_\mathrm{F} M_Z^2$ is dominated by the uncertainty on M_Z^2, which is now 48×10^{-6} [$M_Z = (91\,188.2 \pm 2.2]$ MeV [9]).

- G_F is commonly determined assuming exclusively V-A interactions. A somewhat more general

formula has been given by Greub *et al.* [10]:

$$G_{\rm F}^2 = \frac{192\pi^3\hbar}{\tau_\mu m_\mu^5}\left[1+\frac{\alpha}{2\pi}\left(\pi^2-\frac{25}{4}\right)\right]\left[1-\frac{3}{5}\left(\frac{m_\mu}{m_W}\right)^2\right]$$

$$\times\left[1-4\eta\frac{m_e}{m_\mu}-4\lambda\frac{m_{\nu_\mu}}{m_\mu}+8\left(\frac{m_e}{m_\mu}\right)^2+8\left(\frac{m_{\nu_\mu}}{m_\mu}\right)^2\right], \tag{2}$$

$$\eta = \frac{1}{2}{\rm Re}\left[g_{\rm LL}^{\rm V}g_{\rm RR}^{\rm S*}+g_{\rm RR}^{\rm V}g_{\rm LL}^{\rm S*}+g_{\rm LR}^{\rm V}(g_{\rm RL}^{\rm S*}+g_{\rm RL}^{\rm T*})+g_{\rm RL}^{\rm V}(g_{\rm LR}^{\rm S*}+g_{\rm LR}^{\rm T*})\right], \tag{3}$$

$$\lambda = \frac{1}{2}{\rm Re}\left[g_{\rm LL}^{\rm S}g_{\rm LR}^{\rm S*}+g_{\rm RR}^{\rm S}g_{\rm RL}^{\rm S*}-2g_{\rm RR}^{\rm V}g_{\rm RL}^{\rm V*}-2g_{\rm LL}^{\rm V}g_{\rm LR}^{\rm V*}\right]. \tag{4}$$

Here, besides the muon lifetime and the muon mass, radiative corrections to first order and mass terms are included. Most important is the muon decay parameter η which is 0 in the SM. If we assume that only one additional interaction contributes to muon decay, then $\eta \simeq \frac{1}{2}{\rm Re}g_{\rm RR}^{\rm S}$, where $g_{\rm RR}^{\rm S}$ corresponds to a scalar coupling with right-handed charged leptons. Including the experimental value of $\eta = (-7\pm13)\times10^{-3}$ [11] the error on $G_{\rm F}$ increases by a factor of 20.

2.3 Precision measurement of the Michel parameters

The measurement of individual decay parameters alone generally does not give conclusive information about the decay interaction owing to the many different couplings and interference terms. An example is the spectrum Michel parameter ϱ. A precise measurement yielding the V–A value of 3/4 by no means establishes the V–A interaction. In fact, *any* interaction consisting of an arbitrary combination of $g_{\rm LL}^{\rm S}$, $g_{\rm LR}^{\rm S}$, $g_{\rm RL}^{\rm S}$, $g_{\rm RR}^{\rm S}$, $g_{\rm RR}^{\rm V}$ and $g_{\rm LL}^{\rm V}$ will yield exactly $\varrho = 3/4$ [12]. This can be seen if we write ϱ in the form [13]:

$$\varrho - \tfrac{3}{4} = -\tfrac{3}{4}\left\{|g_{\rm LR}^{\rm V}|^2+|g_{\rm RL}^{\rm V}|^2\right\}+2\left(|g_{\rm LR}^{\rm T}|^2+|g_{\rm RL}^{\rm T}|^2\right)+Re\left(g_{\rm LR}^{\rm S}g_{\rm LR}^{\rm T*}+g_{\rm RL}^{\rm S}g_{\rm RL}^{\rm T*}\right). \tag{5}$$

For $\varrho = \frac{3}{4}$ and $g_{\rm RL}^{\rm T} = g_{\rm LR}^{\rm T} = 0$ (no tensor interaction) one finds $g_{\rm RL}^{\rm V} = g_{\rm LR}^{\rm V} = 0$, with all of the remaining six couplings being arbitrary! On the other hand, any deviation from the canonical value certainly would signify new physics. Tree-level new physics contributions to the Michel parameters occur in supersymmetric theories with R-parity violation or theories with left–right symmetric gauge groups. For instance, the R-parity violating interactions $\lambda_{311}L_{\rm L}^{(3)}L_{\rm L}^{(1)}\bar{E}_{\rm R}^{(1)}+\lambda_{322}L_{\rm L}^{(3)}L_{\rm L}^{(2)}\bar{E}_{\rm R}^{(2)}$ (where the index denotes the lepton generation) give the following contributions [14]

$$\Delta\rho = \frac{3\epsilon^2}{16},\ \ \Delta\eta = \frac{\epsilon}{2},\ \ \Delta\xi = -\frac{\epsilon^2}{4},\ \ \Delta\delta = 0,\quad \epsilon \equiv \frac{\lambda_{311}\lambda_{322}}{4\sqrt{2}G_{\rm F}\tilde{m}^2_{e_{\rm L}^{(3)}}}. \tag{6}$$

For a left–right model, one finds

$$\Delta\rho = -\frac{3}{2}\vartheta_{W_{\rm R}}^2,\ \ \Delta\xi = -2\vartheta_{W_{\rm R}}^2-2\left(\frac{M_{W_1}}{M_{W_2}}\right)^4, \tag{7}$$

where $\vartheta_{W_{\rm R}}$ is the $W_{\rm L}$–$W_{\rm R}$ mixing angle, and M_{W_1} (M_{W_2}) is the mass of the mainly left (right) charged gauge boson. Measurements of ϱ and ξ with a precision of 10^{-4} can probe $W_{\rm R}$ masses of about 1 TeV (in the most unfavourable case $\vartheta_{W_{\rm R}} = 0$) and values of the R-parity violating couplings $\lambda_{311} \approx \lambda_{322} \approx 0.2$ (for a slepton mass of 200 GeV). These tests are competitive with direct searches at high-energy colliders.

There exist also observables which yield valuable information even if they assume their canonical values, all of which are related to the spin variables of the muon and the electron:

- A measurement of the decay asymmetry yields the parameters δ and $P_\mu\xi$. Especially interesting is the combination $P_\mu\xi\delta/\varrho$, which has been measured at TRIUMF [15] with a precision of $\approx 3\times10^{-3}$. A new, ambitious experiment measuring ϱ, δ and $P_\mu\xi$ is currently under construction at TRIUMF [16].

- A measurement of the longitudinal polarisation of the decay electrons P_L consistent with 1 yields limits for all five couplings where the electrons are right-handed. This is a difficult experiment due to the lack of highly polarised electron targets used as analysers. The present precision is $\Delta P_\mathrm{L} = 45\times10^{-3}$.

- The angular dependence of the longitudinal polarisation of decay positrons at the endpoint energy is currently being measured at PSI by the Louvain-la-Neuve–PSI–ETH Zürich Collaboration [17]. This yields the parameter ξ'' which is sensitive to the right-handed vector and the tensor currents.

- A measurement of the transverse polarization of the decay positrons requires a highly polarised pulsed muon beam. From the energy dependence of the component P_{T_1} one can deduce the low-energy decay parameter η which is needed for a model-independent value of the Fermi coupling constant. The second component P_{T_2}, which is transverse to the positron momentum and the muon polarisation, is non-invariant under time reversal. A second generation experiment performed at PSI by the ETH Zürich–Cracow–PSI Collaboration has just finished data-taking [18, 19]. The expected experimental errors are $\Delta P_{\mathrm{T}_1} = \Delta P_{\mathrm{T}_2} = 5\times10^{-3}$.

2.4 Experimental prospects

As mentioned above, the precision on the muon lifetime can presumably be increased over the ongoing measurements by one order of magnitude. Improvement in measurements of the decay parameters seems more difficult. Most ambitious is the TRIUMF project which will soon start taking data and thereby improve the parameters ϱ (positron energy spectrum), $P_\mu\xi$ and δ (decay asymmetry) by more than one order of magnitude. The limits on most other observables are not given by the muon rates which usually are high enough already ($\approx 3\times10^8$ s^{-1} at the μE1 beam at PSI, for example), but rather by effects like positron depolarisation in matter or by the small available polarisation ($< 7\%$) of the electron targets used as analysers. The measurement of the transverse positron polarisation might be improved with a smaller phase space (lateral beam dimension of a few millimetres or better). This experiment needs a *pulsed* beam with high polarisation.

3 SEARCH FOR MUON NUMBER VIOLATION

3.1 Theoretical considerations

In the Standard Model (SM), muon number is exactly conserved. When neutrino masses are added and neutrino oscillations take place, muon-number violating processes involving charged leptons become possible as well. However, because of the smallness of neutrino masses, the rates for these processes are unobservable [20, 21]; for instance

$$B(\mu\to e\gamma) = \frac{3\alpha}{32\pi}\sum_i \left| V^*_{\mu i}V_{ei}\frac{m^2_{\nu_i}}{M^2_W}\right|^2 \sim 10^{-60}\left|\frac{V^*_{\mu i}V_{ei}}{10^{-2}}\right|^2\left(\frac{m_{\nu_i}}{10^{-2}\ \mathrm{eV}}\right)^4 . \tag{8}$$

The observation of muon number violation in charged muon decay would, therefore, serve as an unambiguous sign of new physics and indeed, a number of SM extensions may be probed sensitively by the study of rare muon decays. Here we will concentrate on supersymmetric models and models with extra dimensions, but it should be pointed out that various other SM extensions also predict observable rates for the rare μ decays, like models with new Z$'$ gauge bosons [22], leptoquarks [23] or Lorentz-invariance violation [24, 25]. For a recent review on muon number violation, see Ref. [26].

We first present a model-independent formalism for studying rare muon decays and for comparing the rates of the different muon-number-violating channels. Then, we discuss predictions for the branching ratios of rare muon processes in extensions of the SM with low-energy supersymmetry, in the context of the seesaw mechanism and grand unification, both with and without the conservation of R parity. Finally, we present the expectations in models with extra dimensions.

3.1.1 Model-independent analysis of rare muon processes

Although a purely model-independent analysis based on effective operators cannot make any prediction for the absolute rate of rare muon processes, it can be very useful in determining the relative rates. We will compare the rates for $\mu^+ \to e^+\gamma$, $\mu^+ \to e^+e^-e^+$, and μ^-–e^- conversion. In a large class of models, the dominant source of individual lepton number violation comes from a flavour non-diagonal magnetic-moment transition. Let us therefore consider the effective operator

$$\mathcal{L} = \frac{m_\mu}{\Lambda^2}\bar{\mu}_R\sigma^{\mu\nu}e_L F_{\mu\nu} + \text{h.c.} \tag{9}$$

This interaction leads to the following results for the branching ratios of $\mu^+ \to e^+\gamma$ ($B(\mu \to e\gamma)$) and $\mu^+ \to e^+e^-e^+$ ($B(\mu \to 3e)$), and for the rate of μ^-–e^- conversion in nuclei normalised to the nuclear capture rate ($B(\mu N \to eN)$):

$$B(\mu \to e\gamma) = \frac{3(4\pi)^2}{G_F^2\Lambda^4}\,, \tag{10}$$

$$\frac{B(\mu \to 3e)}{B(\mu \to e\gamma)} = \frac{\alpha}{3\pi}\left(\ln\frac{m_\mu^2}{m_e^2} - \frac{11}{4}\right) = 6\times 10^{-3}\,, \tag{11}$$

$$\frac{B(\mu N \to eN)}{B(\mu \to e\gamma)} = 10^{12}\,B(A,Z)\,\frac{2G_F^2 m_\mu^4}{(4\pi)^3\alpha} = 2\times 10^{-3}\,B(A,Z)\,. \tag{12}$$

Here $B(A,Z)$ is an effective nuclear coefficient which is of order 1 for elements heavier than aluminium [27]. The logarithm in Eq. (11) is an enhancement factor for $B(\mu \to 3e)$, which is a consequence of the collinear divergence of the electron-positron pair in the $m_e \to 0$ limit. Nevertheless, because of the smaller phase space and extra power of α, $B(\mu \to 3e)$ and $B(\mu N \to eN)$ turn out to be suppressed with respect to $B(\mu \to e\gamma)$ by factors of 6×10^{-3} and $(2\text{–}4)\times 10^{-3}$, respectively. This should be compared with the experimental sensitivities for the different processes, discussed in the next subsections.

Next, let us include an effective four-fermion operator which violates individual lepton number

$$\mathcal{L} = \frac{1}{\Lambda_F^2}\bar{\mu}_L\gamma^\mu e_L \bar{f}_L\gamma_\mu f_L + \text{h.c.}\,, \tag{13}$$

where f is a generic quark or lepton. The choice of the operator in Eq. (13) is made for concreteness, and our results do not depend significantly on the specific chiral structure of the operator. First we consider the case in which f is neither an electron nor a light quark, and therefore $\mu^+ \to e^+e^-e^+$ and μ^-–e^- conversion occur only at the loop level. Comparing the $\mu^+ \to e^+\gamma$ rate in Eq. (10) with the contributions from the four-fermion operator to $B(\mu \to 3e)$ and $B(\mu N \to eN)$, we find

$$\frac{B(\mu \to 3e)}{B(\mu \to e\gamma)} = \frac{8\alpha^2 N_f^2}{9(4\pi)^4}\left(\frac{\Lambda}{\Lambda_F}\right)^4\left[\ln\frac{\max(m_f^2,m_\mu^2)}{M_F^2}\right]^2\,, \tag{14}$$

$$\frac{B(\mu N \to eN)}{B(\mu \to e\gamma)} = 10^{12}\,B(A,Z)\,\frac{32G_F^2 m_\mu^4 N_f^2}{9(4\pi)^6}\left(\frac{\Lambda}{\Lambda_F}\right)^4\left[\ln\frac{\max(m_f^2,m_\mu^2)}{M_F^2}\right]^2\,. \tag{15}$$

Here N_f is the number of colours of the fermion f and M_F is the heavy-particle mass generating the effective operators (typically M_F is much smaller than Λ or Λ_F because of loop factors and mixing

angles). The logarithms in Eqs. (14) and (15) correspond to the anomalous dimension mixing of the operator in Eq. (13) with the four-fermion operator generating the relevant rare muon process [28]. If $\Lambda \sim \Lambda_F$, then the contributions from the four-fermion operator are irrelevant, since the ratios in Eqs. (11) and (12) are larger than those in Eqs. (14) and (15). More interesting is the case in which the four-fermion operator in Eq. (13) is generated at tree level, while the magnetic-moment transition in Eq. (9) is generated only at one loop, as in models with R-parity violation [14] or with leptoquarks [23]. In this case, we expect

$$\left(\frac{\Lambda}{\Lambda_F}\right)^4 \simeq \frac{(4\pi)^3}{\alpha} \,. \tag{16}$$

If Eq. (16) holds and if we take $M_F \simeq 1$ TeV, then the ratios in Eqs. (14) and (15) become of order unity, so the different rare muon processes have comparable rates.

Alternatively, if the fermion f in Eq. (13) is an electron (or a light quark), the effective operator can mediate $\mu \to 3e$ (or μ^-–e^- conversion) at tree-level, and the corresponding process can dominate over the others [29]. For instance, we obtain

$$\frac{B(\mu \to 3e)}{B(\mu \to e\gamma)} = \frac{1}{12(4\pi)^2}\left(\frac{\Lambda}{\Lambda_F}\right)^4 \,, \tag{17}$$

for the case $f = e$.

Figure 1 summarizes the behaviour of the ratio of branching ratios as a function of the relative strength of the effective operators in Eq. (9) and Eq. (13), when the fermion f in Eq. (13) is an electron, as in the left part of Fig. 1, or a combination of first generation quarks, as in the right part of Fig. 1. It can easily be seen from the plots that when the magnetic moment operator dominates ($\Lambda^2 \ll \Lambda_F^2$) the ratio of branching ratios saturates at several times 10^{-3}, while it grows like $(\Lambda^2/\Lambda_F^2)^2$ when the four-fermion operators are dominant ($\Lambda^2 \gg \Lambda_F^2$). Interference effects are largest when $\Lambda^2 \sim \Lambda_F^2$, as expected.

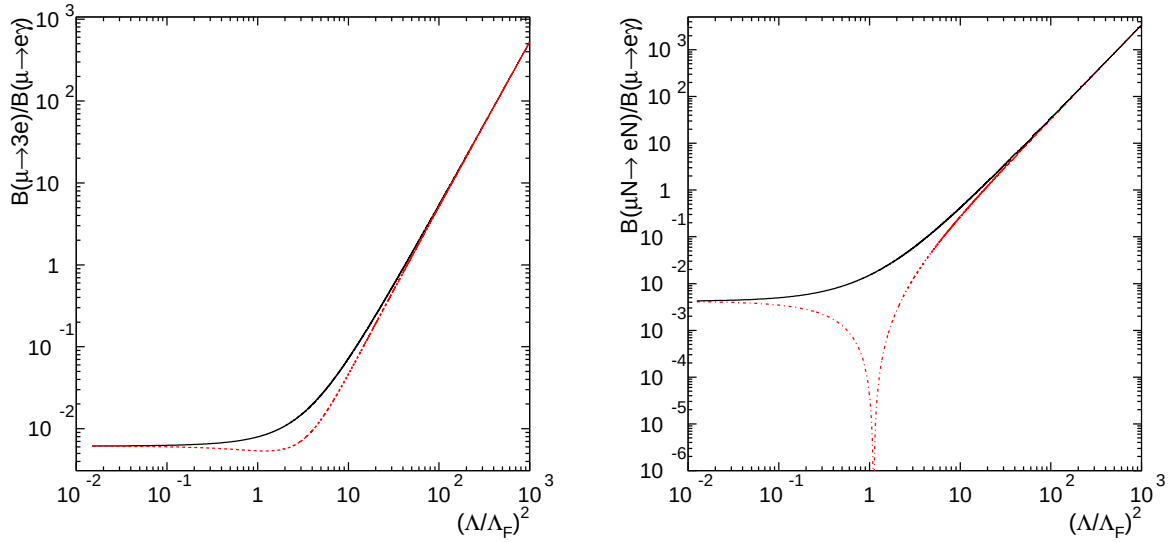

Fig. 1: Branching ratios normalised to $B(\mu \to e\gamma)$ as a function of the ratio of the couplings of effective dimension-5 and dimension-6 operators (see text), for $\mu^+ \to e^+e^-e^+$ (left) and $\mu^- N \to e^- N$ conversion in ^{48}Ti. The solid (dashed) curves apply when the two operators interfere constructively (destructively).

In conclusion, the various rare muon processes are all potentially very interesting. In the event of a positive experimental signal for muon-number violation, a comparison between searches in the different

channels and the use of the effective-operator approach discussed here will allow us to quickly identify the correct class of models.

The study of rare muon decays also allows for the possibility of observing 'weak' time-reversal invariance violation (T violation)[1]. While one cannot construct experimentally accessible T-violating observables in $\mu^+ \to e^+\gamma$ decay, in $\mu^+ \to e^+e^-e^+$ this is a possibility if the muon is polarized [30, 21]. In this case, one may test whether the angular distribution of the decay electrons depends on the T-odd Lorentz invariant $\propto \vec{P}_\mu \cdot (\vec{p}_{e1} \times \vec{p}_{e2})$ (here p_{ei}, $i = 1, 2$ are the momenta of the two positrons in the μ^+ rest frame and $\vec{P}_\mu$ is the muon polarisation). In particular, a T-odd asymmetry can be defined (see Refs. [30, 31] for details). In a number of theoretical models (see Refs. [31, 29, 32] and references therein) 'large' values (up to 24% [29]) for this T-odd asymmetry can be obtained. Unfortunately, in these cases the branching ratio for $\mu^+ \to e^+\gamma$ is significantly larger than that for $\mu^+ \to e^+e^-e^+$.

It should also be noted that, again when the decaying muons are polarised, a number of P-odd observables in $\mu^+ \to e^+\gamma$ and $\mu^+ \to e^+e^-e^+$ can be defined. The measurement of these P-odd asymmetries can play a significant role when it comes to distinguishing different classes of models that yield significant flavour violation in the charged lepton sector (see Refs. [31, 29, 32] and references therein).

3.1.2 Rare muon processes in supersymmetry

Supersymmetric extensions of the SM provide a very promising way of rendering the hierarchy of physical mass scales more natural. Moreover, low-energy supersymmetry often leads to large sources of individual lepton number violation. It provides a framework for computing physics observables in a controlled manner as a function of a well-defined set of parameters. Those, in turn, can thus be constrained by the experimental limits. Whereas lepton-flavour number violation in rare μ decays may well have the same source as neutrino oscillations, the rates generically are no longer suppressed by powers of neutrino masses: It is worth recalling that, for large values of the ratio of the two Higgs vacuum expectation values $\tan\beta$, the coefficient of the non-diagonal magnetic-moment operator in Eq. (9) grows linearly with $\tan\beta$ since, at the loop level, the chiral flip can be generated by the Higgs with the larger vacuum expectation value, and thus

$$B(\mu \to e\gamma) \propto \tan^2\beta\,. \tag{18}$$

We distinguish two different supersymmetric sources of lepton-flavour number violation.

• *Flavour non-diagonal soft terms*

It is well known [33] that a mismatch in flavour space between the lepton and slepton mass matrices generates tree-level transitions between different leptonic generations, both in charged and neutral currents. For instance, if we indicate the mixing angle between the first two generations of sleptons schematically by $\theta_{\tilde{e}\tilde{\mu}}$, we obtain

$$B(\mu \to e\gamma) \simeq \frac{\alpha^3 \pi \theta^2_{\tilde{e}\tilde{\mu}}}{G_F^2 \tilde{m}^4}\,, \tag{19}$$

where $\tilde{m}$ is a typical supersymmetric mass. In general, $\theta_{\tilde{e}\tilde{\mu}}$ receives contributions from the flavour mismatches of left- and right-handed sleptons and sneutrinos. Complete formulae for the rates of rare muon processes with the functional dependence on the different supersymmetric parameters can be found in Ref. [34]. As is apparent from Eq. (19), the rates for rare muon processes can be large in supersymmetric models, since $\theta_{\tilde{e}\tilde{\mu}}$ is not necessarily suppressed by powers of neutrino masses.

For generic values of the soft supersymmetry-breaking mass scale $\tilde{m} \sim 1$ TeV, the experimental limits on rare muon decays transform in very stringent upper limits on $\theta_{\tilde{e}\tilde{\mu}}$. Therefore, it is common

[1] It should be kept in mind that the study of CP violation is not practical due to the experimental difficulty of stopping negative muons in matter without absorbing them.

to invoke some universality condition or flavour symmetry that implies $\theta_{\tilde{e}\tilde{\mu}} = 0$ at the scale at which the soft terms are generated. If this scale is sufficiently low, as in gauge-mediated supersymmetry, then loop corrections are small and rare muon processes are unobservable [35]. However, if the scale of supersymmetry breaking is large, as in supergravity models, then at the quantum level the soft terms are corrected by any high-energy flavour-violating interactions, and we generally expect more sizeable slepton mixing angles [36].

For quantitative estimates we consider two examples for flavour-violating interactions at high energy. Both are commonly present in supergravity models. Additional sources of flavour violations should be expected and therefore our estimates should be viewed as conservative lower bounds.

The first mechanism comes from renormalisable Dirac neutrino Yukawa couplings y_ν at energies larger than M_R [34, 37, 38, 39], the scale of the right-handed neutrino masses. Here we are assuming that the smallness of the neutrino masses results from the seesaw mechanism [40]. In the basis in which the charged-lepton Yukawa coupling matrix is diagonal, loop corrections to the slepton mass matrix are not diagonal in flavour space:

$$\left(m^2_{\tilde{\ell}_L}\right)_{ij} \simeq -\frac{3m_0^2 + A_0^2}{8\pi^2}\,(y_\nu)^*_{ki}\,(y_\nu)_{kj}\,\ln\frac{M_{Pl}}{M_R}\ . \tag{20}$$

Here m_0 and A_0 are the universal soft supersymmetry-breaking scalar mass and trilinear term, respectively, and we have assumed that all three right-handed neutrinos have the same mass M_R. The contribution in Eq. (20) induces flavour-violating mixing angles for both sneutrinos and charged sleptons, and therefore rare muon processes are generated by loop diagrams involving charginos and neutralinos.

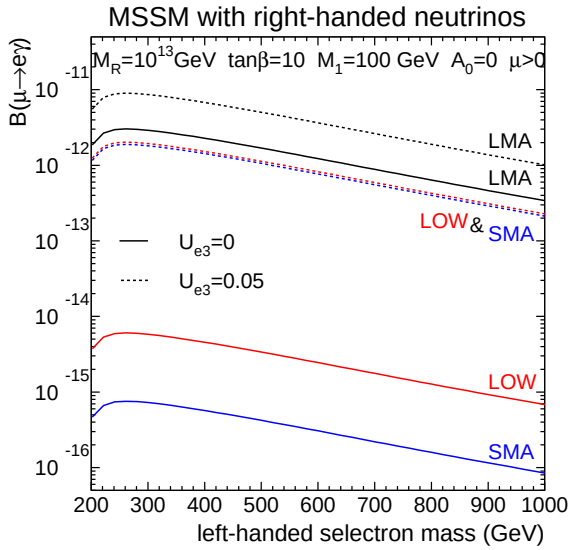

Fig. 2: B($\mu \to e\gamma$) as a function of the left-handed selectron mass for SUSY models with heavy right-handed neutrinos. The assumption here is that the right-handed neutrino mass matrix is proportional to the identity matrix with $M_R = 10^{13}$ GeV, and that all the neutrino mixing comes from the Yukawa couplings. LMA, SMA, and LOW refer to different solutions to the solar neutrino puzzle (see Ref. [41]).

The experimental information on neutrino oscillation parameters [41], is not sufficient to reconstruct the complete structure of the relevant mass matrices. Therefore, it is necessary to rely on specific ansätze for them. Figure 2 depicts the value of $B(\mu \to e\gamma)$ as a function of the left-handed selectron mass, assuming that the right-handed neutrino mass matrix is proportional to the identity and that $M_R = 10^{13}$ GeV. Results are shown for three different solutions to the solar neutrino puzzle and different values of the U_{e3} element of the neutrino mixing matrix (see Ref. [41]), assuming maximal $\nu_\mu \leftrightarrow \nu_\tau$ mixing as the solution to the atmospheric neutrino puzzle. Although the prediction for $B(\mu \to e\gamma)$ can vary significantly, depending on differences in the assumed texture of neutrino masses, supergravity models in which neutrino masses are obtained via the seesaw mechanism can induce $\mu \to e\gamma$ at rates close to the current experimental sensitivity. This is especially true if the solution to the solar neutrino puzzle is indeed the large mixing angle solution or if the U_{e3} element is nonzero. It should be noted, however,

that because the magnitudes of neutrino Dirac Yukawa couplings are related to the right-handed neutrino mass scale M_R in seesaw models, $B(\mu \to e\gamma)$ is very sensitive to the right-handed neutrino scale, roughly

$$B(\mu \to e\gamma) \propto M_R^2 [\ln(M_{Pl}/M_R)]^2 \; . \tag{21}$$

As can be seen in Fig. 2, the prediction for $B(\mu \to e\gamma)$ also depends quite sensitively on the assumed value of U_{e3}. This is a reflection of the general sensitivity to assumptions on the textures of the charged-lepton and neutrino mass matrices.

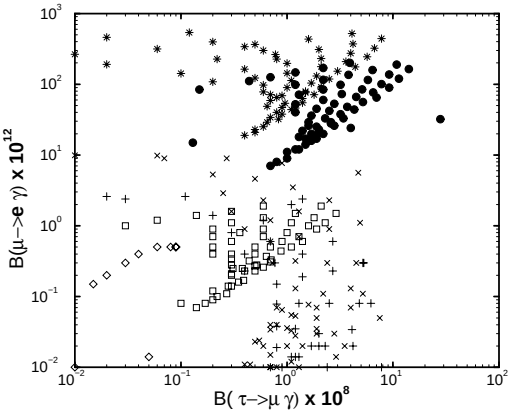

Fig. 3: Scatter plot of values of $B(\mu \to e\gamma)$ and $B(\tau \to \mu\gamma)$ in a sampling of models of lepton masses and mixing with textures generated by $U(1)$ flavour symmetries. There is considerable spread in the predictions, but it seems that $\mu \to e\gamma$ decay may offer better prospects for discovering new physics than does $\tau \to \mu\gamma$, within this class of models [39]. Note that current experiments already constrain $B(\mu \to e\gamma) < 1.2 \times 10^{-11}$ and $B(\tau \to \mu\gamma) < 1.1 \times 10^{-6}$.

Figure 3 displays values of $B(\mu \to e\gamma)$ and $B(\tau \to \mu\gamma)$ found [39] in a sampling of specific models whose masses and mixing angles have different textures generated by $U(1)$ flavour symmetries. We see that the predictions span a considerable range, but, in this class of models, values of $B(\mu \to e\gamma)$ close to the present experimental limit tend to be associated with values of $B(\tau \to \mu\gamma)$ that are considerably below the present experimental upper limit $B(\tau \to \mu\gamma) \sim 10^{-6}$, suggesting that $B(\mu \to e\gamma)$ may be a more promising place to search for new physics. On the other hand, improving the sensitivity to $B(\tau \to \mu\gamma)$ provides very useful information when it comes to disentangling different neutrino mass models [38].

The decay $\mu^+ \to e^+e^-e^+$ is usually dominated by an intermediate photon, and therefore Eq. (11) holds rather generally. This dominance is less certain in $\mu^- – e^-$ conversion, so there may be some deviations from Eq. (12). One particular example [39] is shown in Fig. 4, where the penguin-diagram contribution (which includes the magnetic-moment part) is plotted separately from the sum of penguin and box diagrams. As in Fig. 1, we see that Eq. (12) holds generically to within some numerical factor of order unity.

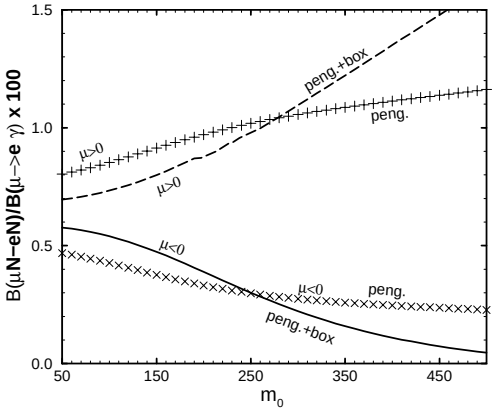

Fig. 4: The ratio of the rates for μ–e conversion and $\mu \to e\gamma$, as a function of m_0 for $\mu > 0$ and $\mu < 0$ ($\tan\beta = 3$) [39]. The penguin contribution, which includes the magnetic-moment piece, is plotted separately from the sum of the penguin and box diagrams. The results are in the range expected from Eq. (12).

The possible discrepancy between the Standard Model and the recent measurement of the muon anomalous magnetic moment $\delta a_\mu \equiv (g_\mu - 2)$ [42] puts a new perspective on the searches for $\mu \to e\gamma$

and related processes. Quite generally, the discrepancy, if confirmed, would be evidence for new physics at the TeV scale that might be detectable in other processes involving muons [43]. Within any specific model that incorporates lepton-flavour violation as inferred from neutrino-oscillation experiments, the magnitude of δa_μ may be used to normalise the prediction for $B(\mu \to e\gamma)$. This correlation is very close if δa_μ is due to supersymmetry [44, 45, 46], since $\mu \to e\gamma$ decay is dominated by the magnetic-dipole-moment type operator in Eq. (9), and the supersymmetric contribution $\delta a_\mu^{\rm SUSY}$ to the muon anomalous magnetic moment is induced by similar diagrams mediated by sleptons, neutralinos and charginos. If the left-handed sleptons have lepton-flavour-violating soft masses, the correlation is particularly strong, since the dominant contributions to both $\mu \to e\gamma$ and $\delta a_\mu^{\rm SUSY}$ are from the left-handed slepton–chargino loop diagrams:

$$\delta a_\mu^{\rm SUSY} \simeq \frac{5\alpha_2^2 + \alpha_Y^2}{48\pi} \frac{m_\mu^2}{m_{\rm SUSY}^2} \tan\beta, \tag{22}$$

$$B(\mu \to e\gamma) \simeq \frac{\pi}{75}\alpha(\alpha_2 + \frac{5}{4}\alpha_Y)^2 (G_{\rm F}^2 m_{\rm SUSY}^4)^{-1} \tan^2\beta \left(\frac{(m^2_{\tilde{\ell}_L})_{12}}{m^2_{\rm SUSY}}\right)^2, \tag{23}$$

$$= 3 \times 10^{-5} \left(\frac{\delta a_\mu^{\rm SUSY}}{10^{-9}}\right)^2 \left(\frac{(m^2_{\tilde{\ell}_L})_{12}}{m^2_{\rm SUSY}}\right)^2. \tag{24}$$

Here we have assumed, for illustration, that all the supersymmetric mass parameters are equal to a common mass, $m_{\rm SUSY}$. Assuming that the 2.6-sigma deviation recently observed in the Brookhaven E821 experiment [42] is due to low energy SUSY, (*i.e.*$\delta a_\mu^{\rm SUSY} \sim 10^{-9}$), we can use the present experimental upper limit $B(\mu \to e\gamma) < 1.2 \times 10^{-11}$ to obtain a stringent constraint on the lepton-flavour-violating mass insertion:

$$\frac{(m^2_{\tilde{\ell}_L})_{12}}{m^2_{\rm SUSY}} \leq 6 \times 10^{-4} \left(\frac{\delta a_\mu^{\rm SUSY}}{10^{-9}}\right)^{-1} \left(\frac{B(\mu \to e\gamma)}{1.2 \times 10^{-11}}\right)^{\frac{1}{2}}. \tag{25}$$

As can be seen from Eq. (20), for example, large neutrino Yukawa couplings could easily induce an observable effect in the near future. The correlation between $B(\mu \to e\gamma)$ and $\delta a_\mu^{\rm SUSY}$ in the case of a specific choice of neutrino mass texture [45], is illustrated in Fig. 5. We see that, at least within the context of this model, $\mu \to e\gamma$ decay may well be observable in the next round of experiments, and the same is true for anomalous $\mu \to e$ conversion on nuclei. The establishment of the anomaly in $g_\mu - 2$, together with improvements of the present experimental limits on rare muon decay processes, will probe severely supersymmetric models.

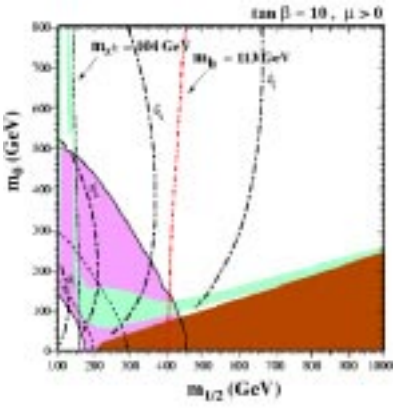

Fig. 5: The contours $B(\mu \to e\gamma) = 10^{-11}, 10^{-12}, 10^{-13}$ and 10^{-14}, for a specific neutrino mass texture described in Ref. [45], in the gaugino ($m_{1/2}$) versus scalar mass (m_0) plane, assuming $\tan\beta = 10$, $A_0 = 0$, and $\mu > 0$. The regions allowed by the E821 measurement of a_μ at the 2-σ level [42] are shaded (pink) and bounded by solid black lines, with dashed lines indicating the 1-σ ranges. The dark (brick-red) shaded regions are excluded because the LSP is the charged stau and the light (turquoise) shaded regions are those with $0.1 < \Omega_\chi h^2 < 0.3$ that are preferred by cosmology. Also shown are the contours $m_h = 113$ GeV (assuming $m_t = 175$ GeV) and $m_{\chi^+} = 104$ GeV.

The second mechanism we investigate is present when the minimal supersymmetric extension of the SM is embedded into a grand unified theory (GUT). In this case, leptons and quarks belong to

the same group representation, and the large top Yukawa coupling y_t will split the mass of the third-generation slepton from the other two [47, 48]. In SU(5) models [49, 50], the up-type quarks are in the same representation as the right-handed charged leptons, and therefore we find

$$\left(m^2_{\tilde{\ell}_R}\right)_{33} \simeq -\frac{3(3m_0^2 + A_0^2)}{8\pi^2} y_t^2 \ln \frac{M_{Pl}}{M_{\rm GUT}} \ . \tag{26}$$

Once the charged-lepton mass matrix is diagonalised, Eq. (26) induces slepton mixing. The left part of Fig. 6 depicts $B(\mu \to e\gamma)$ as a function of the right-handed selectron mass for different values of $\tan\beta$ in the case of an SU(5) GUT. In this case, since the mixing is present only in the right-handed lepton sector, the positron in the anti-muon decay is left-handed, $\mu^+ \to e^+_L\gamma$. This decay could be distinguished from $\mu^+ \to e^+_R\gamma$ by studying the angular distribution of the positron in polarised $\mu^+ \to e^+\gamma$ decays [51, 52].

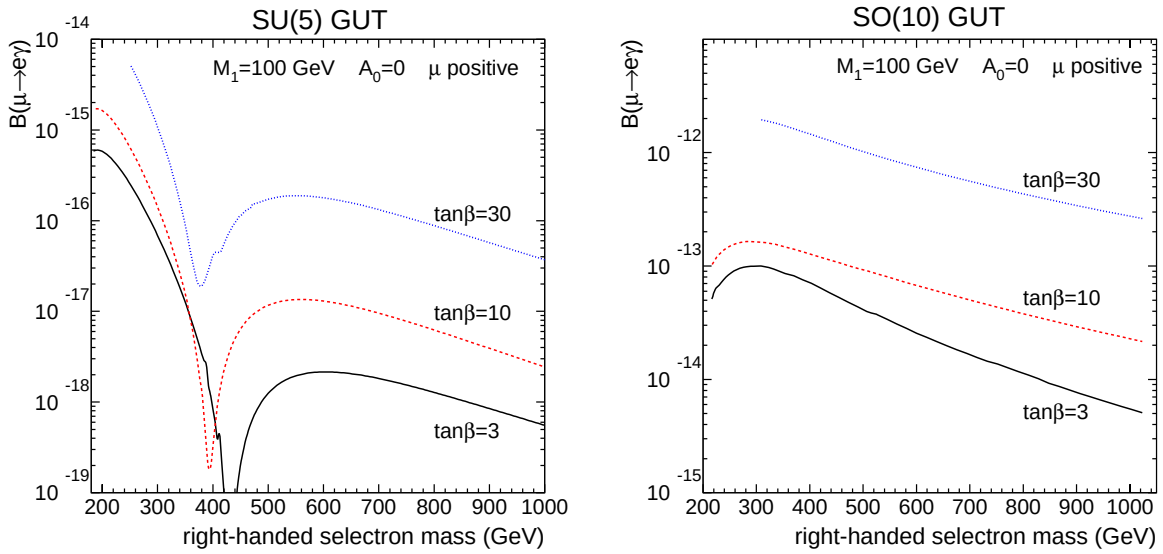

Fig. 6: $B(\mu \to e\gamma)$ as a function of the right-handed selectron mass in supersymmetric models with SU(5) (left) [49] and SO(10) (right) [48] grand unification.

In the case of SU(5) models with massless neutrinos, the rates for $\mu \to e\gamma$ are typically much smaller than the present experimental bound. This is because chargino loop diagrams are absent and neutralino diagrams suffer from a partial cancellation. Note that the position of the dip in the curves of Fig. 6 (corresponding to the exact cancellation) depends on the value of the gaugino mass M_1. However, if higher-dimensional operators are added to models with SU(5) symmetry, $B(\mu \to e\gamma)$ may be enhanced (see, for example, Ref. [50]). Such operators may be required in order to obtain realistic mass relations for first and second generation quarks and leptons. Also note that the values of $B(\mu \to e\gamma)$ depends very strongly on the precise value of the top Yukawa coupling at the GUT scale, which is not well determined by the measurement of the top quark mass, because of its quasi-fixed-point structure.

The situation changes in SO(10) models[2] [48, 54], where all SM fermions belong to the same irreducible representation, and therefore the top Yukawa effect splits not only $\tilde{\ell}_R$, but also $\tilde{\ell}_L$. Furthermore, since the loop diagram involves the exchange of a third-generation slepton, the necessary chiral flip can occur along the $\tilde{\tau}$ line, and $B(\mu \to e\gamma)$ is enhanced by a factor m^2_τ/m^2_μ. Figure 6(right) depicts $B(\mu \to e\gamma)$ as a function of the right-handed selectron mass for different values of $\tan\beta$ in the case of an SO(10) GUT.

[2]Other unification scenarios have also been explored. See, for example, Ref. [53].

• *R-parity violation*

In supersymmetric models where R parity is not imposed as a discrete symmetry, one encounters renormalisable interactions that violate total lepton number and individual lepton numbers. At the scale of the muon mass, these interactions correspond to effective four-fermion operators of the kind discussed in Section 3.1.1. Therefore, depending on the field content of the operator, we can have situations in which $\mu^+ \to e^+e^-e^+$ or μ^-–e^- conversion become the dominant rare muon process. For instance, if a model predicts the simultaneous presence of the two R-parity-violating interactions $\lambda_{131} L_L^{(1)} L_L^{(3)} E_R^{c(1)}$ and $\lambda_{231} L_L^{(2)} L_L^{(3)} E_R^{c(1)}$, then $\mu^+ \to e^+e^-e^+$ occurs at the tree level with a branching ratio

$$B(\mu \to 3e) = \frac{(\lambda_{131}\lambda_{231})^2}{32 G_F^2 m_{\tilde{\nu}_\tau}^4} = \left(\frac{\lambda_{131}\lambda_{231}}{10^{-6}}\right)^2 \left(\frac{200\ \mathrm{GeV}}{m_{\tilde{\nu}_\tau}}\right)^4 10^{-13}\ . \tag{27}$$

Present constraints from rare muon processes provide very stringent upper limits on numerous products of R-parity-violating couplings, some of which are listed in Table 1. At a neutrino factory complex, these bounds could be improved by two orders of magnitude if $\mu \to e\gamma$ and $\mu \to eee$ searches are not successful and by three orders of magnitude if μ–e conversion in nuclei is not observed.

Table 1: Upper limits on products of R-parity-violating couplings from the current limits for muon-number-violating processes, taking slepton masses equal to 100 GeV and squark masses equal to 300 GeV. The values in parentheses indicate the sensitivity which could be achieved at a neutrino factory complex, i.e., resulting from improvements in experimental sensitivities to rare μ decays by 4-6 orders of magnitude. The coupling constants λ and λ' refer to the interactions $W_{\not R} \supset \lambda_{ijk} L^i L^j E^k + \lambda'_{ijk} L^i Q^j D^k$, where i, j, k are generation indices. Tree-level constraints are indicated by [tree].

	$\mu \to e\gamma$	$\mu \to eee$	$\mu \to e$ conversion in nuclei
$\lvert\lambda_{131}\lambda_{231}\rvert$	2.3×10^{-4} (2×10^{-6})	6.7×10^{-7} (7×10^{-9})[tree]	1.1×10^{-5} (1×10^{-8})
$\lvert\lambda_{132}\lambda_{232}\rvert$	2.3×10^{-4} (2×10^{-6})	7.1×10^{-5} (7×10^{-7})	1.3×10^{-5} (2×10^{-8})
$\lvert\lambda_{133}\lambda_{233}\rvert$	2.3×10^{-4} (2×10^{-6})	1.2×10^{-4} (1×10^{-6})	2.3×10^{-5} (3×10^{-8})
$\lvert\lambda_{121}\lambda_{122}\rvert$	8.2×10^{-5} (7×10^{-7})	6.7×10^{-7} (7×10^{-9})[tree]	6.1×10^{-6} (8×10^{-9})
$\lvert\lambda_{131}\lambda_{132}\rvert$	8.2×10^{-5} (7×10^{-7})	6.7×10^{-7} (7×10^{-9})[tree]	7.6×10^{-6} (1×10^{-8})
$\lvert\lambda_{231}\lambda_{232}\rvert$	8.2×10^{-5} (7×10^{-7})	4.5×10^{-5} (5×10^{-7})	8.3×10^{-6} (1×10^{-8})
$\lvert\lambda'_{111}\lambda'_{211}\rvert$	6.8×10^{-4} (6×10^{-6})	1.3×10^{-4} (1×10^{-6})	5.4×10^{-6} (7×10^{-9}) [tree]
$\lvert\lambda'_{112}\lambda'_{212}\rvert$	6.8×10^{-4} (6×10^{-6})	1.4×10^{-4} (1×10^{-6})	3.9×10^{-7} (5×10^{-10}) [tree]
$\lvert\lambda'_{113}\lambda'_{213}\rvert$	6.8×10^{-4} (6×10^{-6})	1.6×10^{-4} (2×10^{-6})	3.9×10^{-7} (5×10^{-10}) [tree]
$\lvert\lambda'_{121}\lambda'_{221}\rvert$	6.8×10^{-4} (6×10^{-6})	2.0×10^{-4} (2×10^{-6})	3.6×10^{-7} (5×10^{-10}) [tree]
$\lvert\lambda'_{122}\lambda'_{222}\rvert$	6.8×10^{-4} (6×10^{-6})	2.3×10^{-4} (2×10^{-6})	4.3×10^{-5} (6×10^{-8})
$\lvert\lambda'_{123}\lambda'_{223}\rvert$	6.9×10^{-4} (6×10^{-6})	2.9×10^{-4} (3×10^{-6})	5.4×10^{-5} (7×10^{-8})

3.1.3 Rare muon processes in models with extra dimensions

Recently, theories with extra spatial dimensions have attracted a lot of attention as a possible solution to the problem of the large hierarchy between the Planck and Fermi mass scales. The hypothesis is that the universe possesses $1 + n$ ($n > 3$) space-time dimensions, while the Standard Model particles are constrained to live on a 1+3-dimensional subspace. Gravity, which is described by the geometry and therefore propagates in the full space, appears very weak to us either because its strength is diluted in a large compactified extra-dimensional space [55] or because it is localised away from us in spaces with non-factorizable geometries [56]. Since these theories assume that gravity becomes strongly coupled at an energy scale M_D comparable to the electroweak scale, the possibility of explaining the smallness

of the neutrino masses via the classical see-saw mechanism is lost. Nevertheless, the small neutrino masses could now have an explanation based on geometrical arguments, similar to those that led to a justification of the small ratio M_W/M_{Pl}. For this to happen, one needs to assume the existence of right-handed neutrinos which, like the graviton, also propagate in the extra dimensions. If this is the case, their Yukawa interactions with the SM left-handed neutrinos are effectively suppressed by large geometrical factors [57], and therefore the SM neutrinos obtain, after electroweak symmetry breaking, a very small Dirac mass. When neutrino family mixing is included, one finds that the Kaluza–Klein modes of the right-handed neutrino mediate, at the loop level, flavour transitions in the charged sector [58, 59].

Particularly interesting are 'minimal models' in which all flavour transitions are described by only two free parameters, besides the observable neutrino masses and mixing angles. These two parameters are the 'fundamental' cut-off scale Λ (expected to be of the order of the weak scale, if these models are motivated by the hierarchy problem) and a dimensionless coefficient ϵ, which is currently constrained to be approximately less than 10^{-2} and whose expected value depends strongly on the neutrino Yukawa couplings and on details of the extra dimensional model, such as the number of extra dimensions δ in which the right-handed neutrinos propagate (see Ref. [59] for details).

Under these conditions, the branching ratio for $\mu \to e\gamma$ is

$$B(\mu \to e\gamma) = \frac{3\alpha}{8\pi}\epsilon^2 \left| U_{e2}U^*_{\mu 2}\frac{\Delta m^2_{\rm sun}}{\Delta m^2_{\rm atm}} + U_{e3}U^*_{\mu 3}\right|^2 \ . \tag{28}$$

Here the unitary matrix U describes the neutrino mixing angles and $\Delta m^2_{\rm sun,atm}$ are the neutrino mass-squared differences relevant to solar and atmospheric oscillation, for a hierarchical neutrino mass spectrum.

Unlike $\ell_i \to \ell_j\gamma$ decays, the rates for $\mu \to eee$ and $\mu \to e$ conversion in nuclei are quite dependent on the unknown ultraviolet details of the models. Nevertheless, these rates can be predicted as a function of ϵ and Λ (see Refs. [58, 59] for complete expressions). It should be noted that the rates for $\mu \to eee$ and $\mu \to e$ conversion in nuclei can be significantly enhanced with respect to the rate for $\mu \to e\gamma$ in some regions of the ϵ, Λ parameter space, similarly to the case of SUSY models with R-parity violation. Figure 7 shows the rates for the different flavour-violating lepton processes, as functions of $|U_{e3}|$, assuming $\Delta m^2_{\rm sun}/\Delta m^2_{\rm atm} = 10^{-2}$, $|U_{\mu 3}/U_{\tau 3}|^2 = 1$, $|U_{e2}/U_{e1}|^2 = 2/3$ (as suggested by atmospheric and LMA solar oscillations), and no CP violation in the neutrino mixing matrix, for different values of ϵ and Λ. We also show the conversion probabilities for $\nu_\mu \to \nu_e$ and $\nu_\mu \to \nu_\tau$ at very short baseline experiments. This allows a comparison of the discovery reach for different facets of a neutrino factory, namely, experiments with stopped muons and experiments with an intense neutrino beam.

We emphasize that the one-loop effects giving rise to rare muon and tau processes that violate individual lepton flavour number are cut-off dependent and can only be qualitatively estimated. Nonetheless, in minimal models, their flavour structure is directly related to the physical neutrino mass matrix, and one is capable of predicting and relating the rates of rare charged and neutral lepton processes in terms of observable neutrino oscillation parameters. This is in sharp contrast to other cases of physics beyond the SM. In SUSY models, for instance, the rates for rare muon processes are perturbatively calculable, but their relations with neutrino oscillations parameters are indirect and strongly model-dependent, as described in the previous subsection.

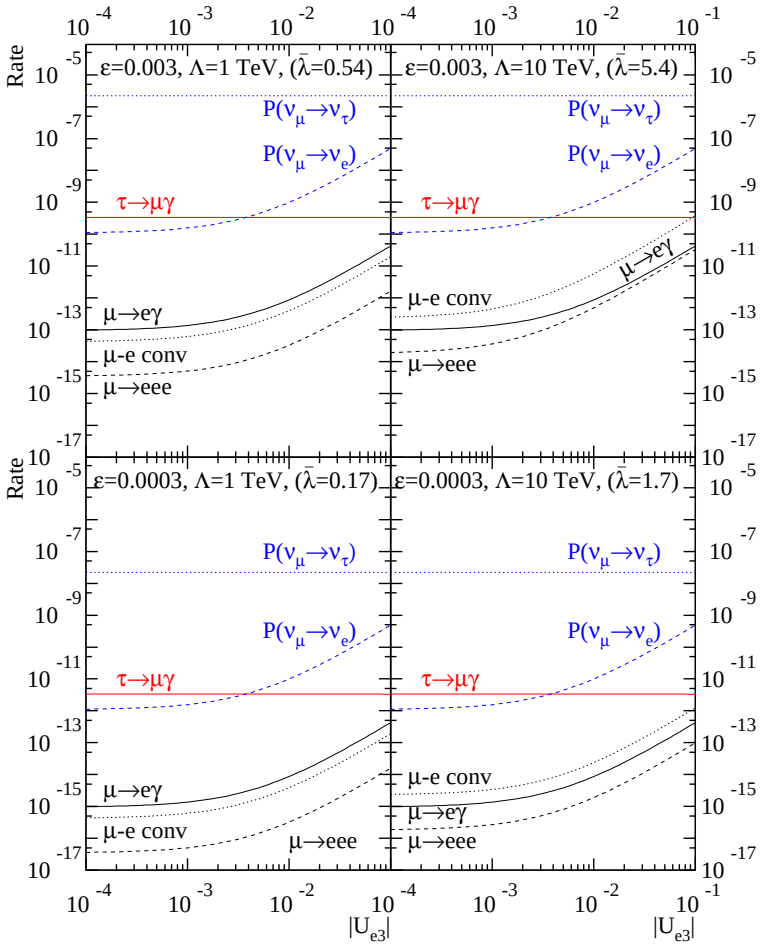

Fig. 7: Branching ratios of $\mu \to e\gamma$, $\mu \to 3e$ and $\tau \to \mu\gamma$, normalized rate of μ–e conversion in ^{27}Al, and transition probabilities for $\nu_\mu \to \nu_\tau$ and $\nu_\mu \to \nu_e$ at very short baseline as functions of $|U_{e3}|$. We have chosen the parameters $\delta = 5$, $\epsilon = 0.003$ (top) or 0.0003 (bottom), and $\Lambda = 1$ TeV (left) or 10 TeV (right). We assumed $\Delta m^2_{\rm sun}/\Delta m^2_{\rm atm} = 10^{-2}$, $|U_{\mu 3}/U_{\tau 3}|^2 = 1$, $|U_{e2}/U_{e1}|^2 = 2/3$ (i.e. maximal mixing in the atmospheric sector and the LMA solution to the solar neutrino puzzle), no CP-violation in the neutrino mixing matrix, and hierarchical neutrino masses ($m_1^2 \ll m_2^2 \ll m_3^2$). See Ref. [59] for details.

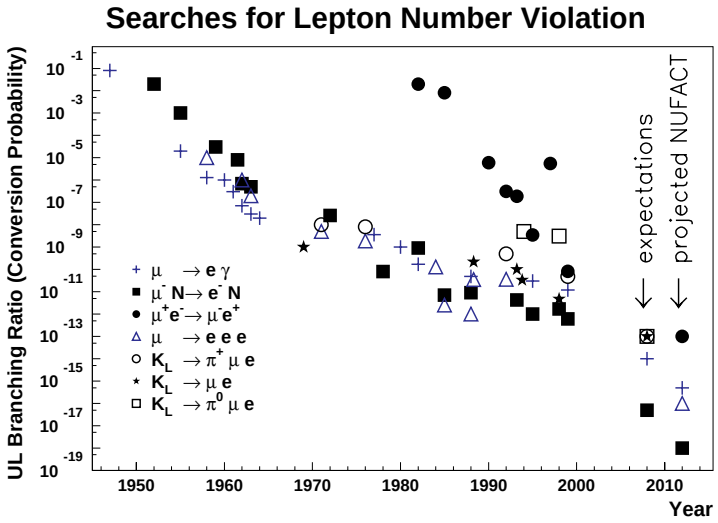

Fig. 8: Historical development of the 90% C.L. upper limits (UL) on branching ratios respectively conversion probabilities of muon-number violating processes which involve muons and kaons. Sensitivities expected for planned searches are indicated in the year 2008 (see also Ref. [26]). The projections for a neutrino factory (NUFACT) are also shown.

3.2 Experimental prospects

The experimental sensitivities achieved during the past decades in tests of muon number conservation are illustrated in Fig. 8. Generally the tests were limited up to now by the intensities of the available μ and K beams, but in some cases detector limitations have played a role as well.

All recent results with μ^+ beams were obtained with 'surface' muon beams [60], i.e. beams of muons originating in the decay of π^+'s that stopped in the pion production target. These beams offer the highest muon stop densities that can be obtained at present, allowing for the low-mass experimental targets that are required for the ultimate resolution in positron momentum and emission angle or the efficient production of muonium in vacuum.

In this subsection we study the question of how far experimental searches could benefit from muon beam intensities which are 2–3 orders of magnitude higher than presently available. We do so by analysing the present state of the art, assuming modest improvements in detector technology.

3.2.1 $\mu \to e\,\gamma$

During the past 25 years the experimental sensitivity to this decay mode was raised by two orders of magnitude (see Table 2). The most sensitive search was performed recently by the MEGA Collaboration, establishing an upper (90% C.L.) limit on $\mathrm{B}_{\mu\to \mathrm{e}\,\gamma}$ of 1.2×10^{-11} [65]. An experiment [66], which aims at a single-event sensitivity of $\sim 10^{-14}$ was approved by the PSI scientific committee in July 1999. Measurements should start in 2003 and data taking should go on for two or three years. This experiment will use a surface muon beam that reaches an intensity around $5 \times 10^8\,\mu^+/s$. As a next step it seems reasonable to consider experiments aiming at a sensitivity of 10^{-15} or better. As we shall see below, it is not at all obvious how to reach such levels of sensitivity without running into the background of accidental $e\gamma$ coincidences.

Table 2: 90% C.L. upper limit on the branching ratio for $\mu \to e\gamma$ obtained by previous experiments at meson factories

Experiment or Lab.	Year	Limit	Ref.
SIN (presently PSI)	1977	1×10^{-9}	[61]
TRIUMF	1977	3.6×10^{-9}	[62]
LANL	1979	1.7×10^{-10}	[63]
Crystal Box	1986	4.9×10^{-11}	[64]
MEGA	1999	1.2×10^{-11}	[65]

Experimental sensitivity

In order to understand how the sensitivity[3] to the $\mu \to e\,\gamma$ decay is related to the experimental resolutions, let us consider an experiment in which muons are stopped in a thin (typically 10 $\mathrm{mg/cm^2}$) target; photons and positrons are detected by a pair spectrometer or an electromagnetic calorimeter and a magnetic spectrometer, respectively. The expected number N_s of observed $\mu \to e\,\gamma$ decays can be written as:

$$N_s = R_\mu T \frac{\Omega}{4\pi} \epsilon_e \epsilon_\gamma \epsilon_{cut}\, \mathrm{B}_{\mu \to \mathrm{e}\,\gamma}\ , \tag{29}$$

where R_μ is the muon stop rate, T is the total measuring time, Ω is the detector solid angle (we assume identical values for the photon and the positron detectors), ϵ_e and ϵ_γ are the positron and photon detection efficiencies, ϵ_{cut} is the efficiency of the selection cuts. Selection cuts can be applied on the reconstructed positron energy (E_e), photon energy (E_γ), opening angle ($\theta_{e\gamma}$) and relative timing ($t_{e\gamma}$). Considering selection windows (indicated with a Δ in front of the relevant quantity) covering 90 % of the signal (full window = 1.4 FWHM for Gaussian distributions) we have $\epsilon_{cut} = 0.9^4 \simeq 0.66$.

The level of prompt background from $\mu^+ \to e^+ \nu \overline{\nu} \gamma$ depends on the selection windows on the energies and opening angle of the $e\gamma$ pair. The background level predicted with no angular cut is shown in Fig. 9. Whereas these estimates do not take into account details of the detector response functions, they are accurate enough for our purpose. It appears that detector technology is sufficiently advanced to keep prompt background at a negligible level

In the proposed PSI experiment (with $R_\mu \simeq 10^8 \mu/\mathrm{s}$) the background is dominated by accidental coincidences of a positron from the normal muon decay and a photon which may originate in the decay $\mu^+ \to e^+ \nu \overline{\nu} \gamma$ or may be produced by an e^+ through external bremsstrahlung or annihilation in flight. In a DC beam the number of accidental coincidences is given by:

$$N_b = {R_\mu}^2 f_e \epsilon_e f_\gamma \epsilon_\gamma (\frac{\Omega}{4\pi})^2\, \pi \frac{\Delta\theta_{e\gamma}^2}{\Omega} 2\Delta t\, T\ , \tag{30}$$

where f_e (f_γ) is the e^+ (γ) yield per stopped muon within the selection window and Δt is the cut applied on the $e^+ - \gamma$ time difference. For a non DC beam N_b must multiplied by the inverse of the duty cycle.

An evaluation of f_e and f_γ is given in Refs. [67, 68]. Figure 10 shows f_γ as a function of the energy threshold calculated for a $50\,\mathrm{mg/cm^2}$ target.

By taking into account the Michel spectrum for the positron and only the radiative muon decay for the photon, one finds near the endpoint (E_e and $E_\mu \simeq m_\mu/2$):

$$f_e \propto \frac{\Delta E_e}{E_e} \qquad f_\gamma \propto (\frac{\Delta E_\gamma}{E_\gamma})^2\ . \tag{31}$$

[3] In this document, sensitivity is defined as the 90% CL upper limit in the absence of a signal.

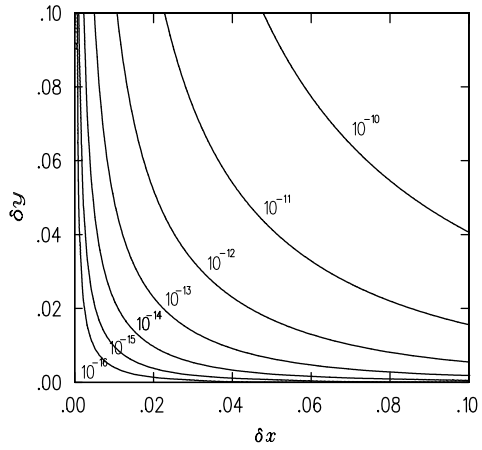

Fig. 9: Prompt background from $\mu^+ \to e^+\nu\overline{\nu}\gamma$ as a function of the selection windows on the positron ($x = 2E_{e^+}/m_\mu$) and photon ($y = 2E_\gamma/m_\mu$) energies. We have defined $\delta x = 1 - x$ and $\delta y = 1 - y$ (results from Ref. [67]).

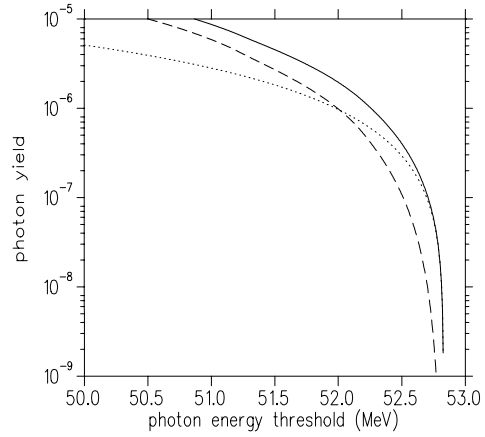

Fig. 10: Photon yield vs. energy threshold. Dotted: annihilation in flight in a $50\,\mathrm{mg/cm^2}$ target. Dashed: radiative decay. Solid: sum of the two.

From Eqs. (29) and (30) the signal-to-background ratio is

$$\frac{N_s}{N_b} = \frac{\epsilon_{cut}\mathrm{B}_{\mu\to\mathrm{e}\,\gamma}}{\mathrm{R}_\mu(\mathrm{f_e f_\gamma}\dfrac{\Delta\theta^2_{\mathrm{e}\gamma}}{4}\,2\Delta\mathrm{t})}\,. \tag{32}$$

The detector resolutions quoted in the PSI proposal are shown in Table 3 together with those of previous experiments. For this experiment a solid angle $\Omega/4\pi$ of about 10% and a total measuring time T of almost a year are being considered. It turns out that one background event is expected and one $\mu \to e\,\gamma$ event for $B_{\mu\to e\,\gamma} = 10^{-14}$.

Since the accidental background rises quadratically with the muon stop rate, it will be even more problematic in future experiments using a higher beam intensity. An experiment with $R_\mu = 10^{10}\mu/\mathrm{s}$ and all the other quantities of Eq. (29) unchanged would yield one $\mu \to e\,\gamma$ event for $B_{\mu\to e\,\gamma} = 10^{-16}$. However, the accidental background would increase to 10^4 events. It is obvious that better detector

Table 3: Detector resolutions, muon stop rates and accelerator duty cycles of the various $\mu \to e\,\gamma$ searches.

Exp./Lab.	$\Delta E_e/E_e$ % FWHM	$\Delta E_\gamma/E_\gamma$ % FWHM	$\Delta t_{e\gamma}$ (ns)	$\Delta\theta_{e\gamma}$ (mrad)	Instantaneous stop rate (1/s)	Duty cycle (%)
SIN (now PSI)	8.7	9.3	1.4	-	$(4\ldots6)\times10^5$	100
TRIUMF	10	8.7	6.7	-	2×10^5	100
LANL	8.8	8	1.9	37	2.4×10^6	6.4
Crystal Box	8	8	1.3	87	4×10^5	$(6\ldots9)$
MEGA	1.2	4.5	1.6	17	2.5×10^8	$(6\ldots7)$
PSI	0.7	1.4	0.15	12	10^8	100

resolutions so as to reduce the product

$$\frac{\Delta E_e}{E_e}\,(\frac{\Delta E_\gamma}{E_\gamma})^2\Delta\theta_{e\gamma}^2\,\Delta t \tag{33}$$

and/or improved experimental concepts are required.

Ideas for background reduction

We report here on some possibilities discussed in the study group.

Detector improvements

The safest improvement can be obtained in the positron momentum resolution where a substantial factor (~ 10) can be gained by utilising a beta-spectrometer [67] which may reach resolutions of the order of 0.1%. As an additional advantage such a spectrometer would result in reduced rates in the tracking detectors as compared to the broad-band systems used so far.

The resolution in $e^+ - \gamma$ opening angle is determined by positron multiple scattering in the stopping target, so another possible improvement could be the reduction of the target thickness. The use of very intense muon beams would give the possibility to obtain a $10^{10}\mu$/s stop rate with much thinner targets. A reduction by one order of magnitude would reduce $\Delta\theta_{e\gamma}$ by a factor of 3, corresponding to an order of magnitude less accidental background, see Eq. (33). Photon background from positron annihilation would be reduced by the same factor. Since the decay $\mu^+ \to e^+\nu\overline{\nu}\gamma$ would then dominate the photon background, one could envisage reducing even this background by vetoing on the accompanying positron.

Target subdivision

Another way to diminish the accidental background could be the use of a row of very thin targets. The requirement for positrons and photons to originate in the same target would reduce the background in proportion to the number of targets. One might think of it as a series of identical $\mu \to e\,\gamma$ set-ups sharing the same beam. However, this configuration poses several complications:

- the photon detector must have sufficient directional selectivity to distinguish between two adjacent targets;
- it is not obvious how to combine the scheme with the idea of a high-resolution positron spectrometer.

Muon polarization

The use of the muon polarization for reducing the accidental background has been suggested in the past [68, 51]. In muon decay, positrons and photons at energies close to the endpoint follow a $(1 + P_\mu \cos\theta)$ angular distribution (where P_μ is the degree of muon polarization). Configurations with back-to-back e^+–γ pairs are therefore suppressed with respect to the unpolarized case. If one requires a reasonable solid angle subtended by the detectors ($\Omega/4\pi \simeq 0.1$) the rejection factor turns out to be approximately 5. It should be noted, however, that in some models $\mu \to e\,\gamma$ would be suppressed as well.

3.2.2 $\mu^+ \to e^+e^+e^-$

From an experimental point of view the decay $\mu \to 3e$ offers some important advantages compared to the more familiar $\mu \to e\gamma$ discussed in the previous section. Since the final state contains only charged particles there is no need for an electromagnetic calorimeter with its limited performance in terms of energy and directional resolution, rate capability, and event definition in general. Apart from the obvious constraints on relative timing and total energy and momentum, as can be applied in $\mu \to e\gamma$ searches as well, there are powerful additional constraints on vertex quality and location to suppress the accidental background. Of major concern, however, are the high rates in the tracking system which has to stand the load of the full muon decay spectrum.

The present experimental limit, $B(\mu \to 3e) < 1 \times 10^{-12}$ [69], was published in 1988. Since no new proposals exist for this decay mode we shall analyse the prospects of an improved experiment with this SINDRUM experiment as a point of reference. A detailed description of the experiment may be found in Ref. [70].

Data were taken during a period of six months in the years 1984 and 1986 when a 25 MeV/c subsurface beam was brought to rest in a hollow double-cone target at a rate of $6 \times 10^6\,\mu^+$ s^{-1}. The target geometry is described in Table 4. The spectrometer acceptance for $\mu \to 3e$ was 24% of 4π sr (for

Table 4: SINDRUM I target for $\mu \to 3e$

Shape	hollow double-cone
Material	foam
Length	220mm
Diameter	58mm
Mass/cm^2	11mg/cm^2
Total mass	2.4 g

a constant transition-matrix element) so the only place for a significant improvement in sensitivity would be the beam intensity. SINDRUM I is a solenoidal spectrometer with a relatively low magnetic field of 0.33 T corresponding to a transverse-momentum threshold around 18 MeV/c for particles crossing the tracking system. This system consists of five cylindrical MWPCs concentric with the beam axis. Three-dimensional space points are found by measuring the charges induced on cathode strips oriented $\pm 45°$ relative to the sense wires. Gating times were typically 50 ns.

Figure 11 shows the time distribution of the recorded $e^+e^+e^-$ triples. Apart from a prompt contribution of correlated triples one notices a dominant contribution from accidental coincidences involving low-invariant-mass e^+e^- pairs. These are explained by Bhabha scattering of positrons from normal muon decay $\mu \to e\nu\overline{\nu}$. The accidental background thus scales with the target mass, but it is not obvious how to reduce this mass significantly from the 11 mg/cm^2 shown in Table 4.

Figure 12 shows the vertex distribution of prompt events. One should keep in mind that most of the uncorrelated triples contain e^+e^- pairs coming from the target and their vertex distribution will thus

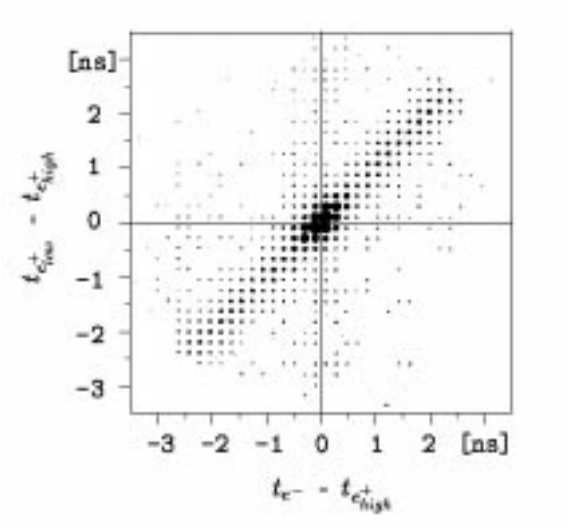

Fig. 11: Relative timing of $e^+e^+e^-$ events. The two positrons are labelled according to the invariant mass when combined with the electron. One notices a contribution of correlated triples in the centre of the distribution. These events are mainly $\mu \to 3e\nu\overline{\nu}$ decays. The concentration of events along the diagonal is due to low-invariant-mass e^+e^- pairs in accidental coincidence with a positron originating in the decay of a second muon. The e^+e^- pairs are predominantly due to Bhabha scattering in the target.

follow the target contour as well. This 1-fold accidental background is suppressed by the ratio of the

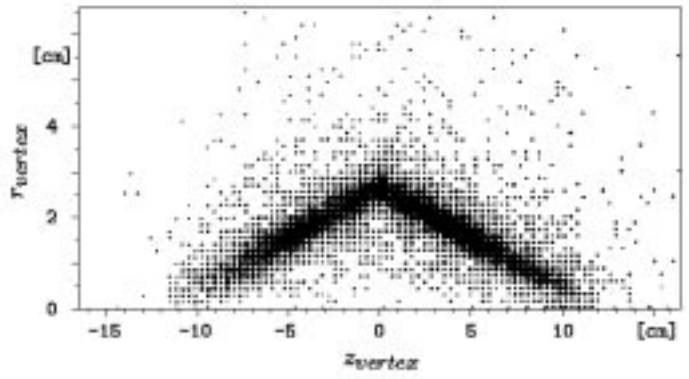

Fig. 12: Spatial distribution of the vertex fitted to prompt $e^+e^+e^-$ triples. One clearly notices the double-cone target.

vertex resolution (couple of mm^2 ?) and the target area. There is no reason, other than the cost of the detection system, not to choose a much larger target than that given in Table 4. Such an increase might also help to reduce the load on the tracking detectors.

For completeness, Fig. 13 shows the distribution of total momentum versus total energy for three classes of events, (i) uncorrelated $e^+e^+e^-$ triples, (ii) correlated $e^+e^+e^-$ triples, and (iii) simulated $\mu \to 3e$ decays. The distinction between uncorrelated and correlated triples has been made on the basis of relative timing and vertex as discussed above.

What would a $\mu \to 3e$ set-up look like that would aim at a single-event sensitivity around 10^{-16}, i.e., would make use of a beam rate around 10^{10} μ^+/s? The SINDRUM I measurement was background-free at the level of 10^{-12} with a beam of 0.6×10^7 μ^+/s. Taking into account that background would

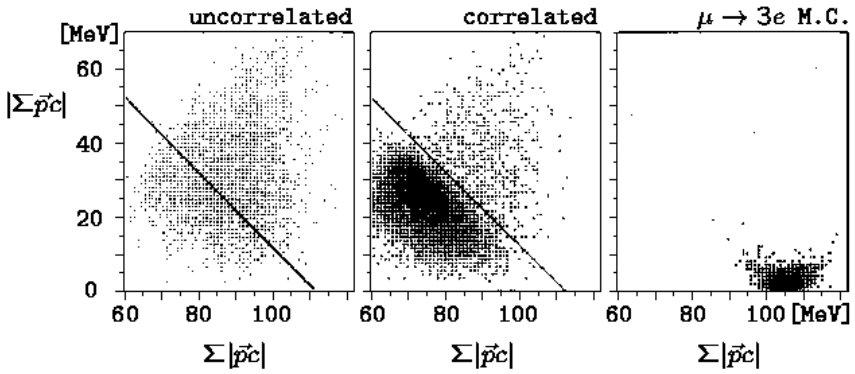

Fig. 13: Total momentum versus total energy for three event classes discussed in the text. The line shows the kinematic limit (within resolution) defined by $\Sigma|\vec{p}c| + |\Sigma\vec{p}c| \leq m_\mu c^2$ for any muon decay. The enhancement in the distribution of correlated triples below this limit is due to the decay $\mu \to 3e\nu\overline{\nu}$.

have set in at 10^{-13}, the increased stop rate would raise the background level to $\approx 10^{-10}$, so six orders of magnitude in background reduction would have to be achieved. Increasing the target size and improving the tracking resolution should bring two orders of magnitude from the vertex requirement alone. Since the dominant sources of background are accidental coincidences between two decay positrons (one of which undergoes Bhabha scattering) the background rate scales with the momentum resolution squared. Assuming an improvement by one order of magnitude, i.e., from the $\approx 10\%$ FWHM obtained by SINDRUM I to $\approx 1\%$ for a new search, one would gain two orders of magnitude from the constraint on total energy alone. The remaining factor 100 would result from the test on the collinearity of the e^+ and the e^+e^- pair.

As mentioned in Ref. [70] a dramatic suppression of background could be achieved by requiring a minimal opening angle (typically 30°) for both e^+e^- combinations. Depending on the mechanism for $\mu \to 3e$, such a cut might, however, lead to a strong loss in $\mu \to 3e$ sensitivity as well.

Whereas background levels may be under control, the question remains whether detector concepts can be developed that work at the high beam rates proposed. A large modularity will be required to solve problems of pattern recognition. Also the trigger for data readout may turn out to be a great challenge.

3.2.3 μe conversion

Neutrinoless $\mu^- \to e^-$ conversion in muonic atoms, $\mu^-(A,Z) \to e^-(A,Z)$ with A mass number and Z atomic number, offers some of the best tests of lepton flavour conservation (LFC). For conversions leaving the nucleus in its ground state the nucleons act coherently, which boosts the conversion probability relative to the rate of the dominant process of nuclear muon capture.

Assuming LFC violation one may wonder how the conversion probability $B_{\mu e}$ varies as a function of Z and A, and with what probability the nucleus stays in its ground state. Earlier calculations [71, 72, 73] predicted a steady rise of the branching ratio until $Z \approx 30$, from where on it was expected to drop again. For this reason most experiments were performed on medium-heavy nuclei. More recently it has been estimated that $B_{\mu e}$ may keep increasing with Z [74, 75]. The same calculations predict the coherent fraction to be larger than 80% for all nuclear systems.

The dependence of $B_{\mu e}$ on the normalized neutron excess $(N-Z)/(N+Z)$, with $N \equiv A - Z$, depends on the nature of the LFC-violating propagator. Although no mechanism considered so far gives rise to a cancellation of the neutron and proton contributions for any given nucleus, a general model-independent analysis requires at least two measurements with significantly different values for $(N-Z)/(N+Z)$ [76, 27].

When negative muons stop in matter, they quickly get captured and form muonic atoms, which mostly reach their ground state before decaying. The main decay channels are muon decay in orbit $\mu^-(A,Z) \rightarrow e^-\overline{\nu}_e\nu_\mu(A,Z)$ and nuclear muon capture $\mu^-(A,Z) \rightarrow \nu_\mu(A,Z-1)$. Experimentally coherent $\mu \rightarrow e$ conversion offers a number of advantages. Since the observation of the process requires the detection of only one particle in the final state, there are no problems with accidental coincidences, which constitute one of the major limitations in searches for $\mu \rightarrow e\gamma$ and $\mu \rightarrow 3e$. The electron is emitted with a momentum $p_e \approx m_\mu c$, which coincides with the endpoint of muon decay in orbit (MIO), which is the only intrinsic background. Since the momentum distribution of muon decay in orbit falls steeply above $m_\mu c/2$ the experimental set-up may have a large geometrical acceptance and the detectors can still be protected against the vast majority of decay and capture events. Energy distributions for MIO electrons have been calculated for a number of muonic atoms [77] and energy resolutions in the order of 1% are sufficient to keep this background below 10^{-16}.

There are several other potential sources of electron background in the energy region around 100 MeV, involving either beam particles or cosmic rays. Beam-related background may originate from muons, pions or electrons in the beam. Apart from MIO, muons may produce background by muon decay in flight or radiative muon capture (RMC). Pions may produce background by radiative pion capture (RPC). Capture gammas from RMC and RPC produce electrons mostly through e^+e^- pair production inside the target.

Beam-related background can be suppressed by various methods:

- Beam pulsing
  Since muonic atoms have lifetimes of order 100 ns, a pulsed beam with buckets short compared to this lifetime would allow one to remove prompt background by measuring in a delayed time window. As will be discussed below there are stringent requirements on the beam suppression during the measuring interval. This is the concept of the new MECO proposal.

- Beam veto
  In the past, prompt background has been removed with the help of a beam counter. For the beam intensities proposed here this method can not be applied.

- Beam purity
  A low-momentum (< 70 MeV/c) μ^- beam with extremely low pion contamination ($< 100\ \pi^-$'s per day) would keep prompt background at a negligible level. A major advantage of the method is that heavy targets such as gold with lifetimes around 70 ns can be studied. This scheme was applied by SINDRUM II and will be discussed in the following.

At present, μe conversion is being searched for by the SINDRUM II Collaboration at PSI [78] and a new experiment (MECO [79]) is planned at BNL. The sensitivity levels are $\approx 5 \times 10^{-13}$ and $\approx 5 \times 10^{-17}$, respectively.

Figure 14 shows the SINDRUM II spectrometer. Beam particles are extracted from a carbon production target at backward angles and momentum-analysed in a conventional quadrupole channel. The beam is focused into a 9 m long transport solenoid (see Fig. 14) called PMC (pion muon converter).

A pion reaching the gold target has a chance of order 10^{-5} to produce an electron in the energy region of interest, so the pion stop rate must be below one every ten minutes. At the PMC entrance the beam contains similar amounts of muons and pions. Since the pion range in matter is about half as large as the corresponding muon range, the pion contamination can be reduced strongly with the help of a moderator at the PMC entrance. Only one out of 10^6 pions may cross this moderator. Typically 99.9% of them would decay before reaching the target. The requirement puts strong constraints on the high-momentum tail transported by the beam line which could be met after a careful optimisation of the beam settings.

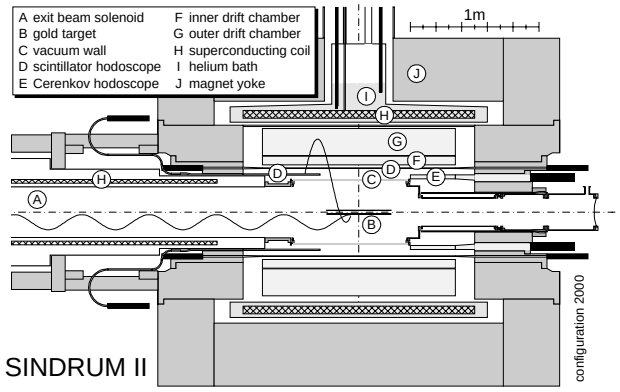

Fig. 14: SINDRUM II

During an effective measuring period of 75 days about 4×10^{13} muons stopped in the gold target. Figure 15 shows as a preliminary result various momentum distributions. The main spectrum, taken at 53 MeV/c, shows the steeply falling distribution expected from muon decay in orbit. Two events were found at higher momenta, but just outside the region of interest. The agreement between measured and simulated positron distributions from μ^+ decay gives confidence in the momentum calibration. At present there are no hints about the nature of the two high-momentum events: they might be induced by cosmic rays or RPC, for example. Both processes result in flat momentum distributions such as shown by the data taken at 63 MeV/c.

As a preliminary result the single-event sensitivity was estimated to be $\approx 2 \times 10^{-13}$, i.e., an improvement by two orders on magnitude of the previous best result on a heavy target [80].

The MECO experiment plans to combat beam-related background with the help of a pulsed 8 GeV/c proton beam. Figure 16 shows the proposed layout. Pions are produced by 8 GeV/c protons crossing a 16 cm long tungsten target, and muons from their decays are collected efficiently with the help of a graded magnetic field. Negatively charged particles with 60–120 MeV/c momenta are transported by a curved solenoid to the experimental target. In the spectrometer magnet a graded field is applied as well. Figure 17 shows the proposed time structure of the proton beam. A major challenge is the requirement for proton suppression in between the proton bursts. In order to keep the pion stop rate in the 'silent' interval below the aforementioned 100 per day, a beam extinction factor better than 10^{-8}–10^{-9} is required.

Table 5 compares the μ^- intensity and single-event sensitivity obtained by SINDRUM II with those expected for MECO and the ν factory.

Two scenarios for a μ^- beam are under study (see also Section 6.2 below):

- A *bunched proton beam* extracted from the accumulator could be used in a fashion similar to the MECO beam line. As explained above, this option requires extinction factors of ten orders of

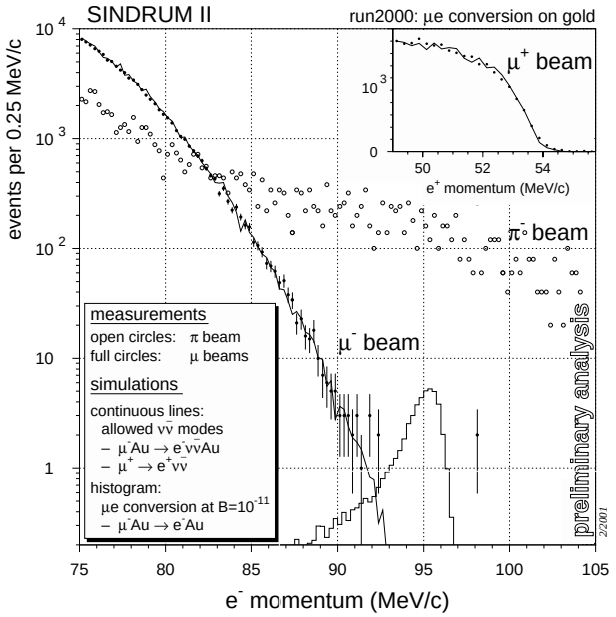

Fig. 15: Recent results by SINDRUM II. Momentum distributions for three different beam momenta and polarities: (i) 53 MeV/c negative, optimised for μ^- stops, (ii) 63 MeV/c negative, optimised for π^- stops, and (iii) 48 MeV/c positive, for μ^+ stops. The 63 MeV/c data were scaled to the different measuring times. The μ^+ data were taken at reduced spectrometer field.

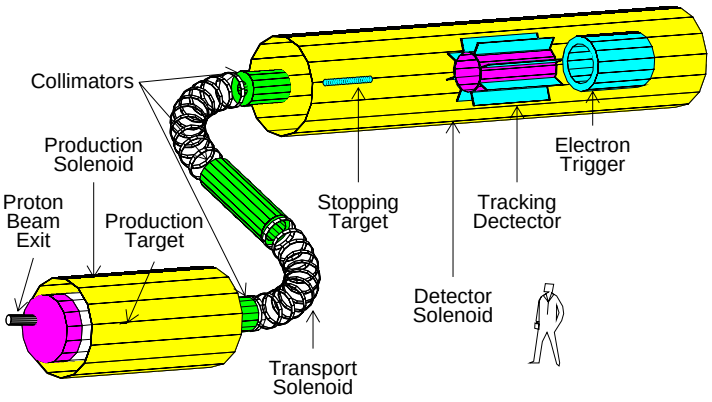

Fig. 16: MECO

magnitude or so to keep prompt background under control.

- As an alternative one might use *a cooled muon beam*. Such a beam would probably be free of pions and contaminated only by decay electrons. As a second by-product of the cooling the extinction factor should be much higher at this stage.

3.2.4 Muonium-antimuonium conversion

Muonium is the atomic bound state of a positive muon and an electron. For leptons a spontaneous conversion of muonium (μ^+e^-) into antimuonium (μ^-e^+) would be completely analogous to the well known $\mathrm{K}^0 - \overline{\mathrm{K}^0}$ oscillations in the quark sector. A search already suggested in 1957 by Pontecorvo [81] three years before the atom was discovered by Hughes [82]. The process could proceed at tree level through bilepton exchange or through various loops. Predictions for the process exist in a variety of speculative models including left–right symmetry, R-parity-violating supersymmetry, GUT theories and several others [83].

Any possible coupling between muonium and its antiatom will give rise to oscillations between

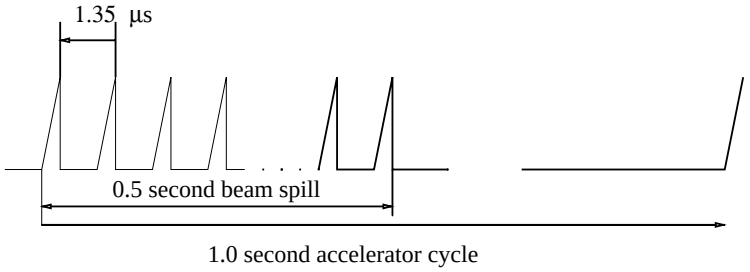

Fig. 17: Proposed beam spill for MECO

Table 5: Rates in μe conversion searches

	SINDRUM II PSI	MECO BNL	NUFACT CERN
Status	Stopped	Proposed	Discussed
Proton momentum [GeV/c]	1.2	8	2
Proton rate [s^{-1}]	1×10^{16}	4×10^{13}	1×10^{16}
μ^- rate [s^{-1}]	3×10^{7}	1.7×10^{11}	10^{14}
μ^- stops [s^{-1}]	$(1 \ldots 2) \times 10^{7}$	1.0×10^{11}	2.0×10^{13}
Single event sensitivity	2×10^{-13}	2.0×10^{-17}	10^{-19}

them. For atomic s-states with principal quantum number n a splitting of their energy levels

$$\delta = \frac{8 G_{\rm F}}{\sqrt{2} n^2 \pi a_0^3} \frac{G_{\rm M\overline{M}}}{G_{\rm F}} \tag{34}$$

is caused, where a_0 is the Bohr radius of the atom, $G_{\rm M\overline{M}}$ is the coupling constant in an effective four-fermion interaction and $G_{\rm F}$ is the weak interaction Fermi coupling constant. For the ground state we have $\delta = 1.5 \times 10^{-12}\,{\rm eV} \times (G_{\rm M\overline{M}}/G_{\rm F})$ which corresponds to 519 Hz for $G_{\rm M\overline{M}} = G_{\rm F}$. An atomic system created at time $t = 0$ as a pure state of muonium can be expected to be observed in the antimuonium state at a later time t with a time dependent probability of

$$p_{\rm M\overline{M}}(t) \quad = \sin^2\left(\tfrac{\delta\, t}{2\,\hbar}\right) e^{-\lambda_\mu t} \quad \approx \left(\frac{\delta\, t}{2\,\hbar}\right)^2 e^{-\lambda_\mu t}\,, \tag{35}$$

where $\lambda_\mu = 1/\tau_\mu$ is the muon decay rate (see Fig. 18). The approximation is valid for a weak coupling as suggested by the known experimental limits on $G_{\rm M\overline{M}}$.

The degeneracy of corresponding states in the atom and its anti-atom is removed by external magnetic fields which can cause a suppression of the conversion and a reduction of the probability $p_{\rm M\overline{M}}$. The influence of an external magnetic field depends on the interaction type of the process. The reduction of the conversion probability has been calculated for all possible interaction types as a function of field strength (Fig. 19) [84, 85]. In the case of an observation of the conversion process, the coupling type could be revealed by measurements of the conversion probability at two different magnetic field values.

The conversion process is strongly suppressed for muonium in contact with matter since a transfer of the negative muon in antimuonium to any other atom is energetically favoured and breaks up the symmetry between muonium and antimuonium by opening up an additional decay channel for the anti-atom only [86] [4]. Therefore any new sensitive experiment needs to employ muonium atoms in vacuum

[4] In gases at atmospheric pressures the conversion probability is approximately five orders of magnitude smaller than in vacuum mainly due to scattering of the atoms from gas molecules. In solids the reduction amounts to even 10 orders of magnitude.

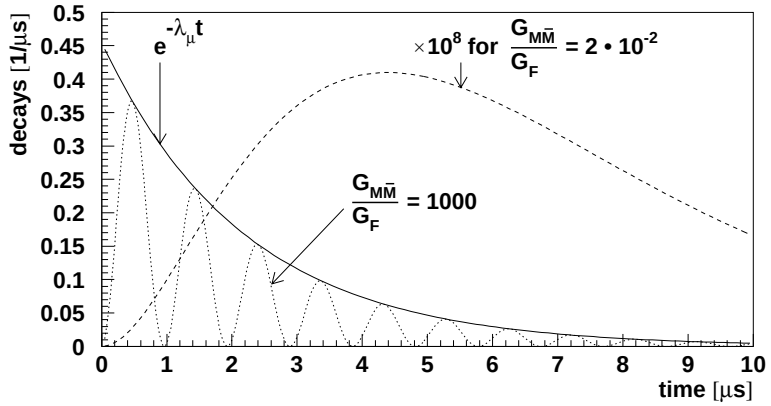

Fig. 18: Time dependence of the probability to observe an antimuonium decay for a system which was initially in a pure muonium state. The solid line represents the exponential decay of muonium in the absence of a finite coupling. The decay probability as antimuonium is given for a coupling strength of $G_{\mathrm{M}\overline{\mathrm{M}}} = 1000 G_F$ by the dotted line and for a coupling strength small compared to the muon decay rate (dashed line). In the latter case the maximum of the probability is always at about 2 muon lifetimes. Only for strong coupling could several oscillation periods be observed.

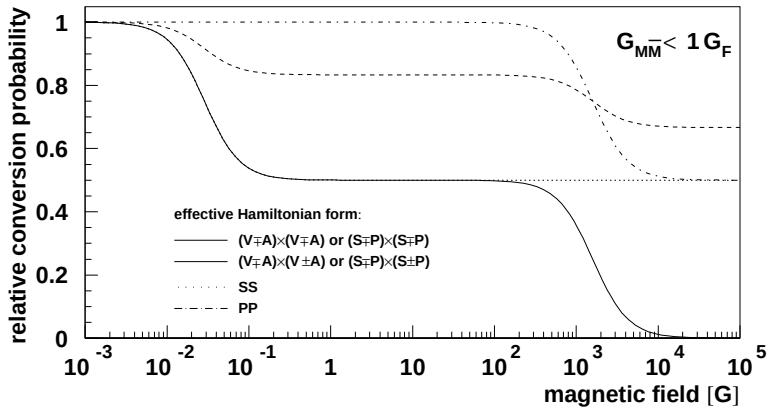

Fig. 19: The muonium to antimuonium conversion probability depends on external magnetic fields and the coupling type. Recent independent calculations were performed by Wong and Hou [84] and Horikawa and Sasaki [85].

[87].

A recent experiment at PSI utilised a powerful signature in which the identification of both constituents of the anti-tom and their coincident detection was requested after its decay. In this an energetic electron appears in the μ^- decay. The positron from the atomic shell remains with an average kinetic energy of 13.5 eV [6]. The energetic particle could be observed in a magnetic wire chamber spectrometer and a position-sensitive microchannel plate (MCP) served as a detector for atomic shell positrons onto which these particles could be transported in a magnetic guiding field after post-acceleration in an electrostatic device. A clean vertex reconstruction and the observation of annihilation γ's in a pure CsI detector surrounding the MCP were required in an event signature [87]. Half a year of actual data-taking was carried out at the currently most intense surface muon source, the πE5 channel at PSI. The previous upper bound on the total conversion probability per muonium atom $P_{\mathrm{M}\overline{\mathrm{M}}} = \int p_{\mathrm{M}\overline{\mathrm{M}}}(t)\mathrm{d}t$ was improved by more than three orders of magnitude and yielded an upper bound of $P_{\mathrm{M}\overline{\mathrm{M}}} \leq 8.0 \times 10^{-11}/S_{\mathrm{B}}$. Here a magnetic field correction S_{B} is included which accounts for the 0.1 T magnetic field in the experimental conditions. It is of order unity and depends on the type of the $\mathrm{M}\overline{\mathrm{M}}$ interaction. For an assumed effective (V–A)×(V–A)-type four-fermion interaction the quoted result corresponds to an upper limit

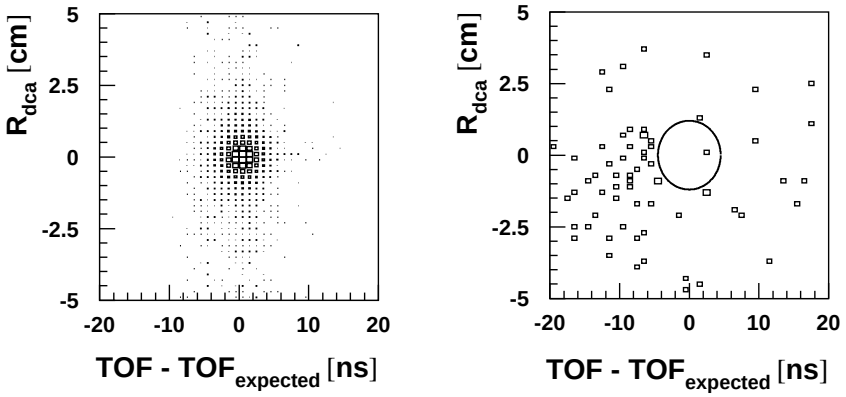

Fig. 20: The distribution of the distance of closest approach (R_{dca}) between a track from an energetic particle in the magnetic spectrometer and the back projection of the position on the MCP detector versus the time of flight (TOF) of the atomic shell particle for a muonium measurement (left) and for all data recorded within 1290 h of data taking while searching for antimuonium (right). One single event falls within 3 standard deviations region of the expected TOF and R_{dca} which is indicated by the ellipse. The events concentrated at early times and low R_{dca}correspond to a background signal from the allowed decay $\mu \to 3e2\nu$. In a new experiment such background could be suppressed significantly through the characteristically different time evolution of a potential antimuonium signal and the background.

for the coupling constant of $G_{\mathrm{M\overline{M}}} \leq 3.0 \times 10^{-3} G_{\mathrm{F}}$ (90 % C.L.). Several limits on model parameters were significantly improved like the mass of the bileptonic gauge boson and some models were strongly disfavoured such as a certain Z_8 model with radiative mass generation and the minimal version of 331 models [87].

With a new and intense pulsed beam the characteristic time dependence of the conversion process could be exploited, if only the decay of atoms that have survived several muon lifetimes τ_μ could be observed. Whereas all beam-muon-related background decays exponentially, the anti-atom population increases quadratically in time giving the signal an advantage over background, which for a 3-fold coincidence signature as in the PSI experiment can be expected to decay with a time constant of $\tau_\mu/3$ [compare Eq. (35)].

Some two orders of magnitude improvement can be envisaged [88] with still no principal background arising from the $\mu \to 3e2\nu$ process or internal Bhabha scattering in which the positron from μ^+ decay would transfer its energy to the electron in the atomic shell and mimic an event which is searched for (Fig. 20).

The requirements forradiation hardness and rate capability of the set-up are similar to those of a $\mu \to 3e$ experiment. As before, a common approach to these two measurements may be found.

3.2.5 Conclusions

All experiments discussed above would benefit from the highest-possible stop-densities, allowing thin targets with minimal distortion of the outgoing particles. In the case of μ^+, most promising are subsurface μ beams that can be stopped in targets of less than a few mg/cm^2.

Better experiments need better detection systems as well. In particular a search for $\mu \to e\,\gamma$ is limited by detector technology and it seems unlikely that the sensitivity will rise in proportion to the beam intensity. Searches for $\mu \to 3e$ and $\mu^+e^- \leftrightarrow \mu^-e^+$ may have similar requirements on the set-up. High granularity will be required for the tracking system which has to stand the load of the full muon decay spectrum.

From the four tests of lepton flavour conservation discussed here, μ-e conversion is expected to

exploit best the increased beam intensity:

- Intrinsic background can be limited to the decay in orbit which can be kept under control by pushing the electron momentum resolution below ≈ 0.5 MeV/c. Care has to be taken to avoid high-momentum components in the momentum response function. Ultimately the resolution would be given by the uncertainty in the energy loss inside the experimental target.
- Detector rates can be kept under control thanks to the steeply-falling transverse momentum distribution.
- Prompt beam-correlated background, in particular induced by pions contaminating the beam, can be removed using a pulsed proton beam. Alternatively, a cooled muon beam might have a sufficiently low pion contamination such that only electrons would have to be suppressed.

In conclusion, all searches would benefit from the projected increase in muon stop rate. In some cases the gain in sensitivity over ongoing experiments might, however, be not more than one order of magnitude.

4 FUNDAMENTAL MUON PROPERTIES

Besides measurements on normal muon decay and the 'classical' searches for the rare decays $\mu \to e\gamma$, $\mu \to eee$, $\mu^- N \to e^- N$ conversion, and muonium-antimuonium conversion (see Section 3.1) which are strongly motivated by our present thinking towards extensions of the Standard Model, there are a number of very interesting experiments on free muons and atomic systems containing muons:

- precise determinations of the properties characterising the muon (e.g. the mass m_μ, magnetic moment μ_μ, magnetic anomaly a_μ, charge q_μ and lifetime τ_μ, see Section 2.2),
- CPT tests from a comparison of μ^- and μ^+ properties,
- measurements of fundamental constants of nature (e.g. the electromagnetic fine structure constant α or the weak interaction Fermi constant G_F),
- sensitive searches for deviations of muon parameters from Standard Model predictions, including novel approaches to search for a permanent muon electric dipole moment edm_μ,
- study of nuclear properties in muonic (radioactive) atoms, and
- applications in condensed matter and life sciences.

In the past most of these topics have been addressed very successfully and in many cases unique information has been extracted. With more intense muon sources they can be accessed with novel and much more precise techniques and substantial progress may be achieved.

4.1 Anomalous magnetic moment of the muon

The anomalous magnetic moment of the muon, $a_\mu \equiv g_\mu - 2$, has been measured in three experiments at CERN, and is presently being measured at BNL [90] (Fig. 21). A superferric precision magnetic field storage ring is employed in which the difference between the spin precession and the cyclotron frequencies is determined. Currently a_μ is experimentally known to 1.3 ppm: $a_\mu^{exp} = 11\,659\,202(14)(6) \times 10^{-10}$ [42].

The most recent and most accurate theory value in the framework of the Standard Model $a_\mu = 11\,659\,159.6(6.7) \times 10^{-10}$ (0.57 ppm) appears to differ from the experimental result by $\Delta a_\mu = 43(16) \times 10^{-10}$ which is about 2.6 times the combined experimental and theoretical uncertainties. Although this

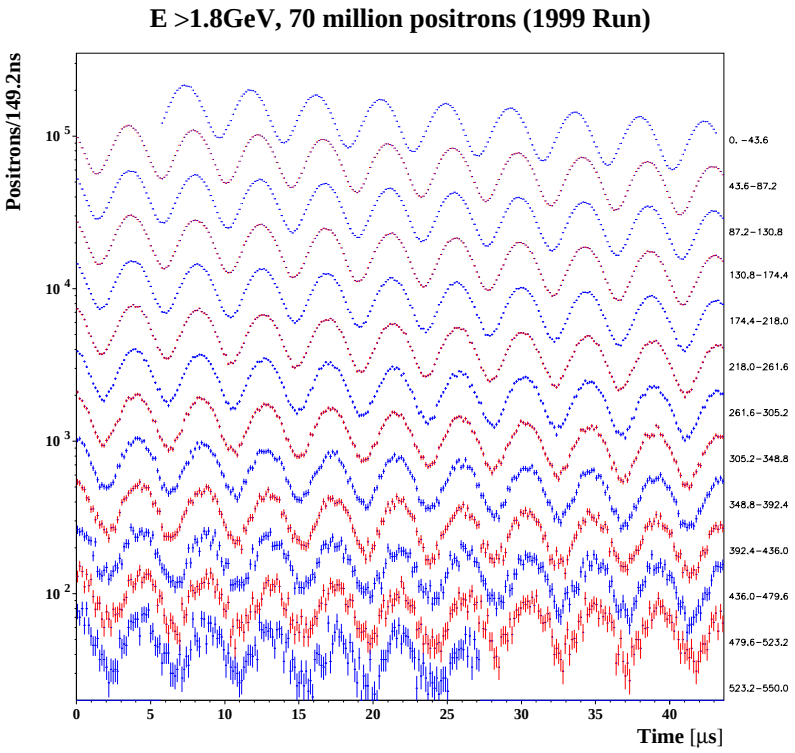

Fig. 21: A sample of new muon $g-2$ data. There is no sign of background after 10 time-dilated muon lifetimes of 64 μs.

discrepancy may be just caused by an underestimate of the uncertainties in the hadronic contributions to the SM value of a_μ, it is also possible that we are facing hints of physics beyond the Standard Model. At this stage, definitive statements cannot yet be made.

Data already recorded at BNL are expected to provide a statistical error for positive muons which is about two times smaller. Data taking with similar accuracy for negative muons is in progress in 2001, with a potential continuation in 2002. Upon completion, this experiment will either provide more confirmed hints of New Physics beyond the Standard Model, or at least limit parameters appearing in speculative models. The large number of models to which $g_\mu - 2$ has some sensitivity includes supersymmetry, lepton compositeness, radiative muon mass models, anomalous W boson parameters, new gauge bosons, leptoquark models, exotic fermions and many more [43].

As examples of where speculations based on the present difference δa_μ may lead, we note that for the constrained minimal supersymmetric extension of the Standard Model (CMSSM) all the preferred parameter space is within reach of the LHC, but may not be accessible to the Tevatron collider, nor to a first-generation $e^+\,e^-$ linear collider with centre-of-mass energy below 1.2 TeV. In many of these models there is a direct connection between a non-standard anomalous muon magnetic moment and other processes discussed in this article. For example, in models with muon substructure, a contribution to a_μ from muon compositeness would suggest that the process $\mu \to e\gamma$ could have a branching ratio above 10^{-13} (see Section 3.1).

From the experimental point of view, the measurements are predominantly statistics-limited. The systematic uncertainties could still be significantly reduced, allowing about one order of magnitude higher accuracy before fundamentally new experimental approaches would be needed. At this point, the present limitations on magnet and field measurement technology as well as particle pile-up would start to impose significant systematic influences on the signal. In order to reduce detector pile-up, a 3.1 GeV short pulsed ($<$100 ns) beam of a few $\times 10$ Hz repetition rate would be most advantageous for a

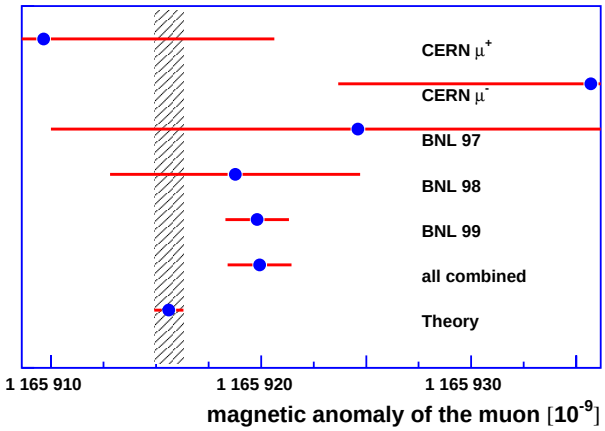

Fig. 22: Comparison of recent measurements of the muon magnetic anomaly with the most accurate and most recent theoretical value [89]. The difference is 2.6 times the combined theoretical and experimental uncertainty.

future experiment. A considerable improvement in accuracy could still be envisaged from a new experimental set-up using a similar approach to the current BNL experiment with a super-ferric storage ring, where the main advantage arises from exploiting higher particle fluxes.

There is, however, a severe limitation to the interpretation of a $g_\mu - 2$ measurement, when seeking to extract or limit parameters of speculative models, namely that due to the hadronic vacuum polarization. Its influence restricts the accuracy of calculations within the Standard Model. Until recently, the hadronic contribution was obtained using a dispersion relation and data from electron-positron annihilation into hadrons, as well as QCD theory. The accuracy of earlier work [91] was improved significantly by newer approaches using hadronic τ decay data [89]. It appears that all newer evaluations agree very well with the newest and most accurate determination and yield an accuracy of better than 0.6 ppm [92, 93]. Newer data for e^+e^- annihilation into hadrons are now available from experiments at Novosibirsk and Beijing and needs to be included. Further improvements can be expected from the DAPHNE accelerator at Frascati, and data on τ decays from B factories may also contribute. However, even if the accuracy of the theoretical value for hadronic vacuum polarisation could be further improved using even higher-quality experimental input, there would still remain an uncertainty arising from the treatment of hadronic light-by-light scattering.

A new and independent $g_\mu - 2$ experiment would undoubtedly be highly desirable if the experiment–theory discrepancy at BNL survives after the experiment is completed.

4.2 Permanent muon electric dipole moment

The identification of new sources of CP violation appears to be a crucial requirement for explaining the dominance of matter over antimatter in the Universe. Permanent electric dipole moments of fundamental particles would violate time reversal (T) invariance and with the assumption of CPT conservation also the CP symmetry.

In the muon $g - 2$ experiment a hypothetical electric dipole moment of the muon edm_μ would cause the plane of its spin precession in the storage ring to be tilted against the plane of its orbit. This inclination can be measured from an asymmetry of the decay electron distribution with respect to the orbital plane. With this method in the latest CERN muon $g - 2$ experiment a limit for edm_μ was established at 1.05×10^{-18} e cm [90]. The ongoing BNL measurements will provide one order of magnitude improvement.

Recently a novel idea was introduced to exploit fully the high motional electric fields in a magnetic storage ring. With an additional radial electric field the spin precession due to the magnetic moment

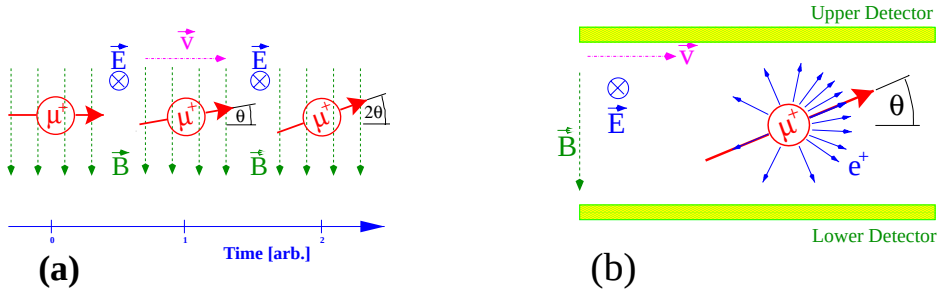

Fig. 23: The basic principle of a novel muon edm experiment. μ^+'s of velocity $\vec{v}$ moving in a magnetic storage ring with field $\vec{B}$ find themselves exposed to a motional electric field $\vec{E} \propto \vec{v} \times \vec{B}$. In case of a finite EDM the muon spin precesses with an angle Θ which grows linearly in time (a), which can be monitored by observing the time dependence of the angular distribution of the decay positrons (b).

anomaly can be compensated. In this case an edm_μ would express itself as a spin rotation angle out of the orbital plane that increases linearly in time (Fig. 23). This can be observed as a time-dependent increase of the above/below plane asymmetry. For the possible muon beams at the AGS synchrotron of BNL a sensitivity of 10^{-24}e cm is expected [94]. In this experiment the possible muon flux is a major limitation. For models with nonlinear mass scaling of edm's such an experiment would already be more sensitive than present experiments on neutral atoms [95]. An experiment carried out at a more intense muon source could provide a significantly more sensitive probe to CP violation in the second generation of particles without strangeness.

It should be noted that the very same experimental technique (and the same experimental set-up) could also be utilized for searching for permanent electric dipole moments of a large variety of relativistic nuclei [96]. Such possibilities were recently explored in a workshop at GSI [97]. Results that are superior to those extracted from present experiments on neutrons or mercury atoms can be expected. Such a novel experiment could be well accommodated at a new and intense ISOL facility associated with the proton machine discussed here.

4.3 CPT tests

In general, any two measurements of muon parameters for both positive and negative muons constitute a CPT test. Such tests were performed for the mass, the magnetic moments and most sensitively for the muon magnetic anomaly. In the framework of a rather general ansatz the past muon g-2 experiments at CERN have provided the best test of CPT invariance at a level of $2 \cdot 10^{-22}$ which is a more than 3 orders of magnitude tighter bound than the mostly quoted $\mathrm{K}^0 - \overline{\mathrm{K}^0}$ mass difference and the value extracted from measurements of the electron and positron magnetic anomalies [25]. From the ongoing measurements of a_μ at BNL one can expect an improvement by at least one order of magnitude in this figure.

5 BOUND MUON SYSTEMS

5.1 Muonic atoms

5.1.1 Muonium

The hydrogen-like muonium atom ($\mathrm{M} = \mu^+ e^-$) is the bound state of a positive muon and an electron [98]. Since both particles may be regarded as structure-less objects with dimensions below 10^{-18} m, their electromagnetic interactions can be calculated to much higher precision than for hydrogen isotopes containing hadrons. In natural hydrogen, for example, the hyperfine structure has been measured six orders of magnitude more accurately than can be calculated because of uncertainties in the proton magnetic radius and polarizability. For muonium the comparison between theory and experiment of this transition could be made with two orders of magnitude higher accuracy than for natural hydrogen. Therefore the

system gives an important input to the set of adjusted fundamental constants [99].

Muonium can be produced most efficiently in the atomic 1s state. For this reason, precision experiments can be carried out on the ground state hyperfine interval and the 1s–2s frequency interval.

Recently an experiment was completed at LAMPF [100] in which two Zeeman transitions in the ground state were induced by microwave spectroscopy. They both involved a muon spin flip and could be detected through a change in the spatial anisotropy of the muon decay positrons. The experiment takes advantage of line narrowing that occurs when only such atoms are detected which have coherently interacted with a microwave field for periods long compared to the average muon lifetime τ_μ ('old muonium' technique [100], Fig. 24). The hyperfine interval was determined to 12 ppb as a test of QED or alternatively as a determination of the fine structure constant α to 58 ppb. The good agreement between this

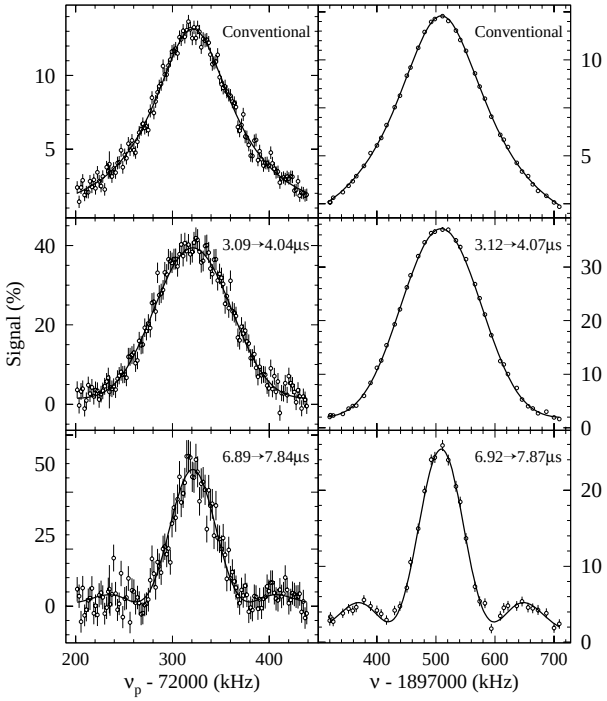

Fig. 24: Muonium hyperfine structure transition signals [100] obtained with magnetic field and with microwave frequency scans using the 'old muonium' technique. Lines of width significantly below the natural width were obtained.

α and the value extracted from a measurement of the electron magnetic anomaly (Fig. 25) is generally interpreted as the best test of internal consistency of quantum electrodynamics. The comparison between theory and experiment is for the muonium hyperfine structure some two orders of magnitude more precise than for electronic hydrogen, where the accuracy of knowledge of the proton magnetic radius and polarizability limit the QED calculations more than seven orders of magnitude below the experiment. In addition, in the measurements the muon magnetic moment (respectively its mass) were determined to 120 ppb.

At RAL the 1s–2s interval was determined to 4 ppb using Doppler-free two-photon spectroscopy with pulsed lasers [102]. The result may be interpreted as a precise muon mass measurement or alternatively as the by far the best test of the charge equality of muon and electron (2 ppb), i.e. two particles from different particle generations. It should be noted that the gauge invariance principle can provide charge quantization only within one particle generation.

The muonium spectroscopy experiments at LAMPF and at RAL were limited largely by statistics only. Systematic errors arising mainly from technical imperfections of the pieces of apparatus involved can be expected to be kept under control for one further order of magnitude gain in accuracy for the hyperfine structure experiment. The laser experiment can be performed with CW lasers and promises some 2–3 orders of magnitude improvement without significant systematics problems, provided 4–5

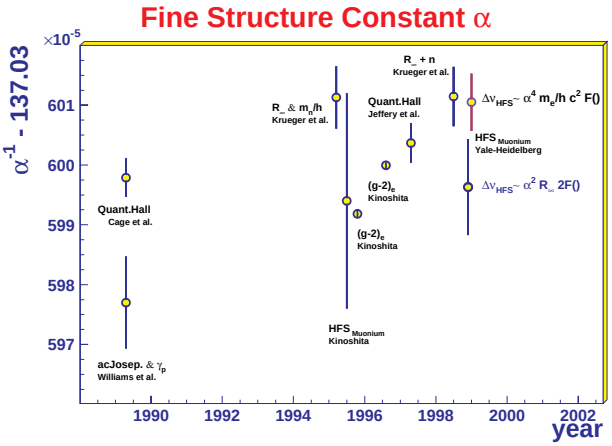

Fig. 25: The fine structure constant α has been determined with various methods (from Ref. [101]). Most precise is the value extracted from the magnetic anomaly of the electron. The muonium atom offers two different routes which use independent sets of fundamental constants. The disagreement (the error bars are mostly statistical) seems to indicate that the uncertainty of h/m_e from neutron de Broglie wavelength measurements may have been underestimated. The degree of agreement between the α values from electron $g-2$ and muonium hyperfine structure is a measure for the internal consistency of quantum electrodynamics and the set of fundamental constants involved in the evaluation.

orders of magnitude increased muon flux is available. In both cases a pulsed time structure would be required.

5.1.2 Radioactive muonic atoms

Muonic atoms have been employed both for testing QED vacuum polarisation and to determine nuclear parameters, most importantly nuclear mean square charge radii.

A novel programme is currently being initiated in a collaboration between various universities and the Paul Scherrer Institute (PSI) in Switzerland and CERN to pursue the possibility to use muonic X-rays to obtain information on very exotic nuclei far from the valley of stability. The exact measurements on muonic X-ray spectra can yield the most precise values for the charge radii of nuclei as well as other ground-state properties such as moments and even B(E2) transition strengths for even–even nuclei. In general, muonic X-rays promise higher accuracy for most of these quantities compared to electron scattering.

The experimental approach proposed is to use ion trapping of exotic isotopes combined with a newly developed muon decelerator concept as well as other muon manipulation techniques of PSI. In this approach, radioactive ions or isotopes capture muons in their outer atomic orbits, subsequently leading to cascade into the inner orbits, resulting in emission of characteristic X-rays of MeV energies due to the increase in binding energies for massive muons. Since the capture is of atomic nature, very high sensitivities are expected for this approach which, if proven successful, would eventually mean one of the greatest new developments in physics of nuclei under extreme conditions. In addition, other physics opportunities offered by muon capture in nuclei will be pursued in this collaboration.

Among the possible scenarios, nested traps for radioactive nuclei and for muons can be envisaged. Large formation rates can be expected from a set-up containing a Penning trap [103] the magnetic field of which serves also for a cyclotron muon trap [104]. For muon energies in the range of electron binding energies the muon capture cross-sections grow to atomic values, efficient atom production can be expected of order 50 systems per second. CERN could be a unique place where such experiments become possible. The ideal beam time structure is the shortest possible pulse with non-specific requirements for repetition rates.

Further, nuclear muon capture in both stable and radioactive muonic atoms offers the possibility to study weak interactions. Of particular interest is the radiative muon capture in hydrogen, where the induced pseudoscalar coupling is a long-standing problem [105].

5.1.3 Muonic hydrogen

In muonic hydrogen [106] the Bohr radius of the system is only 100 times larger than the size of the proton. Therefore electromagnetic transitions in this system are very sensitive to the size and inner structure of the proton. The atom is currently being investigated in an experiment at PSI where the 2s–2p Lamb-shift transition will be induced with infrared laser light [107]. This quantity is mostly determined by QED effects. A significant contribution arises from the proton mean square charge radius the determination of which is the expressed goal of the collaboration at PSI. The proton radius is of significant relevance for electronic hydrogen spectroscopy since it gives a large uncertainty in the interpretation of the observed 1s–2s energy interval. It should be noted that several electron scattering experiments have failed to produce a reliable value of the proton mean square charge radius.

Another important quantity is the hyperfine splitting between the $\mathrm{F} = 0$ and $\mathrm{F} = 1$ states in the μp system. A measurement to an accuracy of 10^{-4} or better would yield new information on the proton polarisability [108]. Such an experiment can be performed with muonic hydrogen atoms produced by depositing a short pulse of muons in the centre of a small cell in which molecular hydrogen gas at high pressure is surrounded by high-Z walls. The average flight time of the system can be measured from the timing of muonic X-rays that are emitted upon arrival of the muonic hydrogen atoms at the wall where immediate muon transfer occurs. The flight time shortens after laser resonance absorption at 6.8 μm wavelength due to the immediate collisional quenching and the 0.12 eV gain in kinetic energy from recoil in this process. Such an experiment would require an intense pulsed beam with less than 500 ns bunch length. If the μ^- beam were polarised the laser transition could be observed as a change in the angular distribution of the decay electrons [106].

5.2 Condensed matter

Muon Spin Rotation and Muon Spin Resonance (μSR) are well-established methods to study bulk condensed matter [109]. A typical μSR experiment requires 10^6 to 10^7 muons. Since any signal is extracted from a spin rotation frequency, the resolution of the apparatus is inversely proportional to the duration of the muon pulse which therefore should be as short as possible.

Efforts are currently under way to produce beams of very slow muons which would make it possible to expand the μSR method to research topics such as surface magnetism, surface diffusion, catalysis. Bio-science applications are currently being explored [110]. They include for example electron transfer mechanisms in proteins. Element analysis at surfaces and in thin layers and membranes through muonic X-rays can be envisaged.

For positive muons, moderation to typically 20$\pm$10 eV (Fig. 26) has been demonstrated [111].

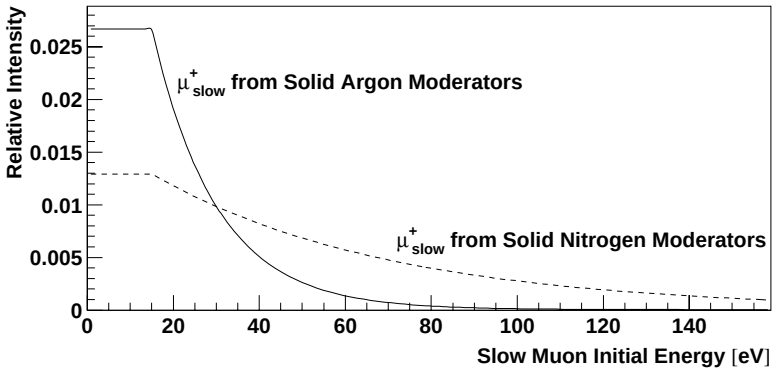

Fig. 26: The energy distributions for slow muons determined for frozen Ar and N_2 targets.

In frozen noble gas targets the particles have negligible interactions with the moderator atoms once

Table 6: Beam requirements for new muon experiments. Given are required sign of charge q_μ and the minimum of the total usable number of muons $\int I_\mu dt$ above which significant progress can be expected in the physical interpretation. The experiments which require pulsed beams (see Fig. 27) are sensitive to the muon suppression I_0/I_m between pulses of length δT and separation ΔT. This does not apply (n/a) for continuous beams. Most experiments require energies below 4 MeV corresponding to 29 MeV/c momentum. Thin targets and storage ring acceptances, demand rather small momentum bites $\Delta p_\mu/p_\mu$.

Experiment	q_μ	$\int I_\mu dt$	I_0/I_m	δT [ns]	ΔT [μs]	E_μ [MeV]	$\Delta p_\mu/p_\mu$ [%]
$\mu^- N \to e^- N^\dagger$	–	10^{21}	$< 10^{-10}$	≤ 100	≥ 1	< 20	< 10
$\mu^- N \to e^- N^\ddagger$	–	10^{20}	n/a	n/a	n/a	< 20	< 10
$\mu \to e\gamma$	+	10^{17}	n/a	n/a	n/a	1...4	< 10
$\mu \to eee$	+	10^{17}	n/a	n/a	n/a	1...4	< 10
$\mu^+ e^- \to \mu^- e^+$	+	10^{16}	$< 10^{-4}$	< 1000	≥ 20	1...4	1...2
τ_μ	+	10^{14}	$< 10^{-4}$	< 100	≥ 20	4	1...10
transvers. polariz.	+	10^{16}	$< 10^{-4}$	< 0.5	> 0.02	30-40	1...3
$g_\mu - 2$	$\pm$	10^{15}	$< 10^{-7}$	≤ 50	$\geq 10^3$	3100	10^{-2}
edm_μ	$\pm$	10^{16}	$< 10^{-6}$	≤ 50	$\geq 10^3$	$\leq$1000	$\leq 10^{-3}$
M_{HFS}	+	10^{15}	$< 10^{-4}$	≤ 1000	≥ 20	4	1...3
M_{1s2s}	+	10^{14}	$< 10^{-3}$	≤ 500	$\geq 10^3$	1...4	1...2
μ^-atoms	–	10^{14}	$< 10^{-3}$	≤ 500	≥ 20	1...4	1...5
condensed matter (incl. bio sciences)	$\pm$	10^{14}	$< 10^{-3}$	< 50	≥ 20	1...4	1...5

† Scenario in which a pulsed beam is utilized.

‡ Scenario in which a continuous beam after the muon cooling stage is employed.

they have reached an energy below the materials band gap. The process which generates such a tertiary muon beam has some 10^{-5} efficiency and requires therefore intense muon sources. The highest flux right now is available at PSI [112].

6 MUON BEAMS

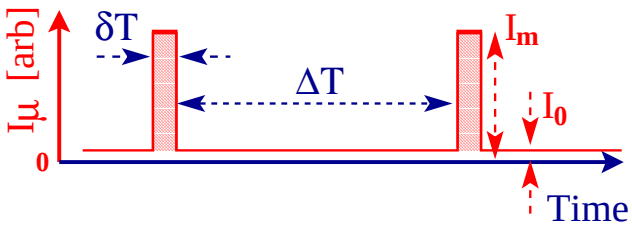

Fig. 27: A pulsed time structure is important for many stopped muon experiments. Crucial parameters are the muon suppression in between the bunches I_0/I_m, the bunch width δT and separation ΔT.

6.1 Beam requirements

The experiments discussed in this report require different types of beam. Measurements with stopped muons require rather low momentum muons with either a pulsed or a continuous time structure. Other

experiments would need higher energy pulsed beams (see Table 6). Continuous (or quasi continuous) beams would be required particularly for experiments with tight coincidence signatures.

Low-momentum positive beams can be obtained up to momenta of $p_s = 29$ MeV/c from so-called 'surface muon' channels [113]. These are beams of muons that originate in the decay of pions that stopped close to the surface of the production target. Their rate increases with $p^{3.5}$ up to a maximum at p_s. Low-momentum negative beams may be obtained from pion decay in the cloud surrounding the production target.

There are important requirements for most experiments on the tolerable momentum bite $\Delta p/p$. This arises from the fact that either only thin targets are possible in which one would like to stop an as high as possible fraction of the beam, or this is determined by the acceptance of subsequent equipment like storage rings. Typically one should aim for $\Delta p/p \approx 1\%$. Muons outside of this band will not be able to contribute to the useful signal, but will most likely contribute to the background.

Muon beams are regularly contaminated by electrons which originate from π_0 decays and pair creation. An essential piece of equipment in a low-energy muon beam line is therefore an electromagnetic separator (Wien filter). The efficiency of such devices is best for low-momentum spread. (They have also an advantage over degrading material, which on the one hand would allow muons to be separated from particles of different masses through different fractional energy losses. On the other hand they would increase the momentum bite.)

6.2 Possible realizations of muon beams

The precise design of muon beams at a neutrino factory complex has not been performed but the following summarises a number of ways by which one could imagine increasing the muon flux by several orders of magnitude over present or foreseen facilities.

The great strength of the CERN-based Neutrino Factory complex as envisaged in the CERN baseline scenario [114], is twofold. Firstly the high intensity offered by the 2.2 GeV/c Superconducting Proton Linac (SPL) [115], which is given to provide 4 MW average power in a 75 Hz pulsed mode or even possibly 24 MW in continuous wave (CW) mode. Secondly, the great flexibility in the beam timing offered by the fact that a proton accumulator and a bunch compressor are foreseen in the complex. These rings are necessary to match the basically continuous time structure of the SPL to the pulsed structure needed to operate the muon acceleration system as well as the storage ring.

Figure 28 shows various locations where targets could be installed along the proton path.

6.2.1 Continuous beams

For experiments requiring a continuous beam ($\mu^+ \to e^+\gamma$, $\mu^+ \to e^+e^+e^-$) two solutions can be envisaged. The benchmark beam for these experiments is the PSI beam for the foreseen $\mu \to e\gamma$ experiment [66].

- An internal target inside the proton accumulator. This solution, shown in Fig. 29, is similar to that sketched in Ref. [116] and it would consist in inserting in the proton accumulator a thin target (typically 1/4000 of an interaction length), either in place of the H^- stripping foil, or elsewhere in the lattice. With respect to the benchmark beam, the gain is obtained from the fact that the beam recirculates many times through the target so that essentially all protons – up to tails generated by large scatters – end up interacting. This gives right away a factor 20 more intensity than the benchmark set-up, where a 5% interaction length target is placed on the proton beam. Since the benchmark beam uses a quadrupole capture system, with the typical aperture of 150 mrad, an additional gain of a factor 40 or so should be achievable with a more efficient capture system, using for instance a solenoidal magnetic field.

  The time structure of the beam is described in Fig. 29. Because the target is very thin, the protons

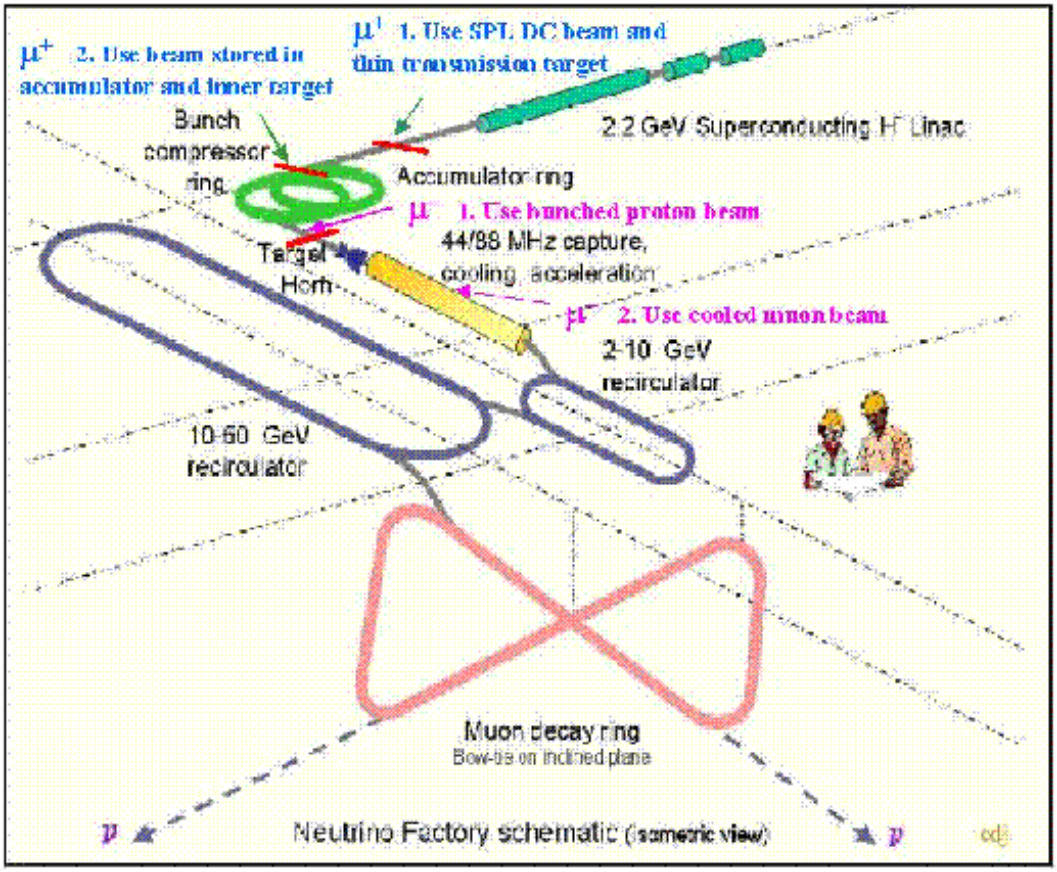

Fig. 28: Possible locations of muon target along the proton path in the CERN neutrino factory baseline scenario.

stay in the accumulator for a long time, and the system behaves as an approximately continuous muon source.

This scheme is currently under evaluation. A serious technical problem to be solved is the design of the target, which will be subject to very intense heating. This can be in principle solved by using a rotating carbon target so that the area of material exposed to the beam (about one square centimetre) is removed and radiation-cooled fast enough as in the PSI E and M targets [117] or in a study for the neutrino factory [118]. Another serious technical problem is the local irradiation around the target area. Since all particles produced in the target, except the muons, will have to be absorbed locally, this will necessitate a very careful design of the area, which receives the same amount of radiation as a beam dump.

- Another possibility would be to use directly the proton beam from the linac operated in high-power, CW mode. This solution is less efficient than the previous one, but could constitute a back-up possibility.

It is therefore seen that improvements due to the target design and capture design, could in principle lead to an increase of the flux by almost three orders of magnitude. This will constitute a considerable opportunity as well as a tremendous challenge to the design of the experiments themselves.

6.2.2 Pulsed beams

Muon conversion experiments, $\mu^- N \rightarrow e^- N$, and various other precision experiments could take significant advantage of a pulsed beam structure (see Table 6 and Fig. 27). A pulsed beam allows a time

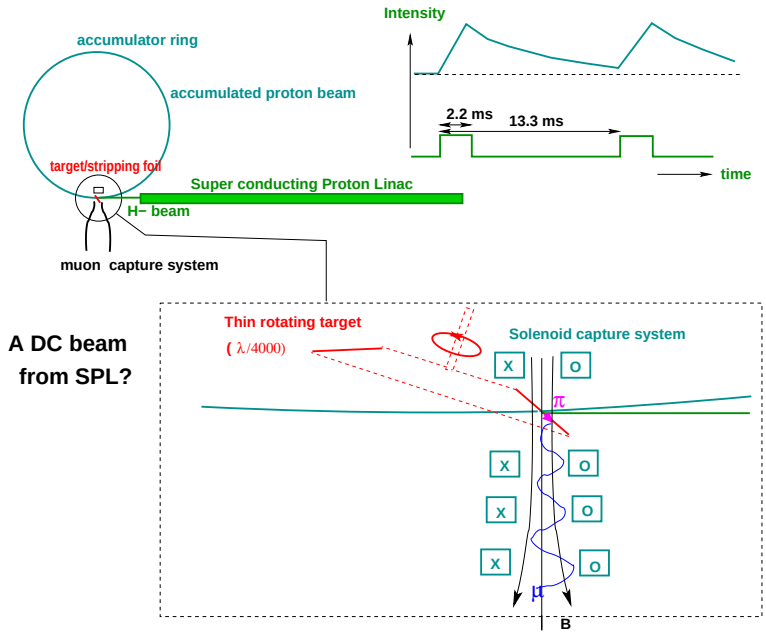

Fig. 29: Sketch of a thin muon production internal target for a quasi-continuous muon beam.

delay of many pion lifetimes to reduce the pion contamination. For this rejection to be efficient, a time separation of a microsecond between pulses is desirable. Two possibilities come to mind.

One could choose to place the production target in a proton beam line at the exit of the buncher. Taking advantage of the SPL timing flexibility, the bunches could in principle be delivered for this application at a frequency different from the nominal one.

Another interesting possibility would be to take advantage of the main muon cooling channel, in which the particles travel for typically 300 metres, ensuring an efficient clean-up from the pions. The muons have a rather broad energy spectrum (typically 200 MeV with an energy spread of 5%) at that level, however, and the stopping power may be limited.

To conclude this section on possible beams, it can be said that the SPL together with its accumulator and buncher rings offers attractive possibilities. A conceptual design and more precise performance estimates of target and beam lines for muon physics at the SPL is now necessary.

7 CONCLUSIONS

The main conclusion of this study is that the physics potential of a new slow muon facility, such as the one that will become available as a necessary step on the way to building a muon storage ring (Neutrino Factory), is very rich and compelling, with a large variety of applications in many fields of basic research. Indeed, muon physics, that has already played an important role in establishing the Standard Model of particle physics, may provide us with crucial information regarding the theory that lies beyond, proving itself to be still far from having exhausted its potential.

This new low-energy muon source will have unprecedented intensity, three to four orders of magnitude larger than presently available. It can have the large degree of flexibility necessary to satisfy the requirements of very different experiments, providing muon beams with a wide variety of momenta and time structures. Both continuous and pulsed beams are possible. In addition, it is capable of producing physics results at the very early stages of the Muon Complex, well before the completion of muon cooling, acceleration, and storage sections.

Only preliminary ideas on the design of this facility are introduced here, suggesting ways by which the muon flux could be boosted orders of magnitude above present or foreseen facilities. The

tasks of detailed conceptual design of target and capture systems and of quantitative estimates of beam performances are still entirely ahead of us. It will be now enthusiastically tackled in view of the physics rewards that are to be expected.

A major interest in muon physics lies in the search for rare processes that violate muon number conservation. In many extensions of the Standard Model, such as supersymmetry, they may occur at rates close to the current experimental bounds. Their discovery would have far-reaching consequences. The most interesting processes are $\mu^+ \to e^+\gamma$, $\mu^+ \to e^+e^-e^+$, and μ^-–e^- conversion in nuclei. We emphasise that all the different processes should be pursued. Indeed, the relative rates of the different modes provide a powerful tool for discriminating different manifestations of new physics. The muon facility discussed here has enough flexibility to allow the study of different muon processes, and promises to be more sensitive by at least a few orders of magnitude, when compared with current experiments.

Experimental prospects on these muon number-violating processes and on the related process of muonium–antimuonium conversions can be summarised as follows:

- The present upper limit on $\mu^+ \to e^+\gamma$ (1.2×10^{-11}) is expected to be reduced (or the process observed), by 2005, to $\sim 10^{-14}$. Exploiting the higher intensities available at a neutrino factory complex is a nontrivial challenge here, as the main limitation to improving the sensitivity to $\mu^+ \to e^+\gamma$ comes from the severe background of accidental coincidences. A number of paths in detector design, aiming at a sensitivity below $\sim 10^{-15}$, are suggested for further exploration.

- The reduction in background necessary to improve the sensitivity to $\mu \to 3e$ beyond the current upper limit $B(\mu \to 3e) < 1 \times 10^{-12}$ appears to be an easier task, if detectors working at the high beam rates proposed can be developed. Sensitivity to $B(\mu \to 3e) > 1 \times 10^{-16}$ or better seems to be attainable.

- The limit on neutrinoless $\mu^- \to e^-$ conversion nuclei is expected to be pushed from the present 6.1×10^{-13} down to 1×10^{-13} soon, while future experiments may be sensitive to conversion probabilities down to 1×10^{-16}. As the experimental sensitivity is completely dominated by the performance of the (pulsed) muon beam, this mode should continue to benefit from increased beam intensity, and conversion probabilities of 1×10^{-18} or smaller could be within reach.

- Muonium–antimuonium conversion could be further probed by using a pulsed beam and taking advantage of the time evolution of the conversion process. One may reach sensitivities to conversion probabilities as small as 10^{-13}, almost three orders of magnitude beyond the present limit of 8.1×10^{-11}. Detector requirements closely resemble those for $\mu \to 3e$ searches.

Normal muon decay can also be studied with increased precision. The muon lifetime could be measured with a precision which is ten times higher than achieved in the ongoing PSI experiments. Improvements on the measurements of decay parameters, via a number of other observables related to the muon and electron spin variables, are also possible but are not limited by muon rates, and appear less promising in view of the current efforts at TRIUMF and PSI.

Several other experiments on free muons and atomic systems containing muons also promise substantial progress:

- A new dedicated muon $g-2$ experiment could improve the experimental precision by almost a factor 15 compared with present experiments, and by almost a factor of 5 compared with the precision expected to be reached by the ongoing BNL experiment (0.35 ppm). This effort may become particularly worthwhile if the recently reported discrepancy is confirmed, although hadronic contributions limit the accuracy of the theoretical prediction. It should also be noted that systematic effects on the magnetic field become important at the level of 0.1 ppm.

Table 7: Experiments which could beneficially take advantage of the intense future stopped-muon sources at the CERN neutrino factory (NUFACT)

Type of experiment	Physics Issues	Possible experiments	Previously established accuracy	Present activities (proposed accuracy)	Projected for NUFACT @ CERN
'Classical' rare & forbidden decays	Lepton Number Violation; Searches for New Physics: SUSY, L-R Symmetry, R-parity violation,.....	$\mu^- N \to e^- N$ $\mu \to e\gamma$ $\mu \to eee$ $\mu^+ e^- \to \mu^- e^+$	6.1×10^{-13} 1.2×10^{-11} 1.0×10^{-12} 8.1×10^{-11}	PSI, proposed BNL (5×10^{-17}) proposed PSI (2×10^{-14}) completed 1985 PSI completed 1999 PSI	$< 10^{-18}$ $< 10^{-15}$ $< 10^{-16}$ $< 10^{-13}$
Muon decays	G_F; Searches for New Physics; Michel Parameters	τ_μ transv. Polariz.	18×10^{-6} 2×10^{-2}	PSI (2x), RAL (1×10^{-6}) PSI, TRIUMF (5×10^{-3})	$< 10^{-7}$ $< 10^{-3}$
Muon moments	Standard Model Tests; New Physics; CPT Tests T- resp. CP-Violation in 2nd lepton generation	$g_\mu - 2$ edm_μ	1.3×10^{-6} $3.4 \times 10^{-19} e$ cm	BNL (3.5×10^{-7}) proposed BNL ($10^{-24} e$ cm)	$< 10^{-7}$ $< 5 \times 10^{-26} e$ cm
Muonium spectroscopy	Fundamental Constants, μ_μ,m_μ,α; Weak Interactions; Muon Charge	M_{HFS} M_{1s2s}	12×10^{-9} 1×10^{-9}	completed 1999 LAMPF completed 2000 RAL	5×10^{-9} $< 10^{-11}$
Muonic atoms	Nuclear Charge Radii; Weak Interactions	μ^- atoms	depends	PSI, possible CERN ($< r_p >$to 10^{-3})	new nuclear structure
Condensed matter	surfaces, catalysis bio sciences ...	surface μSR	n/a	PSI, RAL (n/a)	high rate

- A search for a permanent muon electric dipole moment (edm) would be a fundamentally novel experiment. It could reach a sensitivity similar to or better than present neutron edm searches, down to 5×10^{-26} e cm.

- Muonium microwave and laser spectroscopy could provide more precise measurements of important fundamental constants like the muon mass, the muon magnetic moment, and the electromagnetic fine structure constant. Improvements by one to two orders of magnitude are possible.

- The combination of intense muon beams and a new ISOL facility offer new physics opportunities. Measurements on muonic atoms of radioactive isotopes would reveal properties of nuclei with half-lifes down to milliseconds. One can envisage unknown effects in nuclear structure, comparable to the recent discovery of halo nuclei.

- Muonic hydrogen spectroscopy allows measurements of the proton charge radius with much better accuracies than what is reached in electron scattering experiments.

There are also applications in other fields, such as condensed matter physics and life sciences. Slow muon beams with four orders of magnitude more flux than the most intense sources at PSI are expected to yield new insight in a variety of areas, including surface science, thin films, the chemistry of catalysis and dynamical processes in biological molecules.

We find the discussed experiments theoretically well motivated and capable of providing answers to urgent questions in fundamental physics. The described experiments appear technically feasible at the projected accuracies (Table 6,7). In due time, new international collaborations should be encouraged to work on detailed proposals for the possible experiments with forefront detector technology. We enthusiastically recommend to continue efforts towards designing the new stopped muon facility, and we are ready to fully support the CERN management in its efforts to achieve such a unique physics opportunity.

References

[1] L. Michel, Proc. Phys. Soc. **A63** (1950) 514.

[2] W. Fetscher, H.-J. Gerber and K.F. Johnson, Phys. Lett. **B173** (1986) 102.

[3] P. Langacker, Comm. Nucl. Part. Phys. **19** (1989).

[4] W. Fetscher and H.-J. Gerber, Eur. Phys. J. **C15** (2000) 316.

[5] F. Scheck, in *Electroweak and Strong Interactions* (Springer Verlag, 1996).

[6] W. Marciano, Phys. Rev. **D60** (1999) 093006.

[7] J. Kirkby *et al.*, PSI proposal R-99-06 (1999) and D.W. Hertzog *et al.*, PSI proposal R-99-07 (1999).

[8] K. Nagamine *et al.*, RIKEN-RAL muon lifetime experiment (1998).

[9] D.E. Groom *et al.*, (Particle Data Group), Eur. Phys. J. **C15** (2000) 1.

[10] C. Greub, D. Wyler and W. Fetscher, Phys. Lett. **B324** (1994) 109.

[11] H. Burkard *et al.*, Phys. Lett. **B160** (1985) 343.

[12] W. Fetscher, Phys. Rev. **D42** (1990) 1544.

[13] H.J. Gerber, in *Proceedings of the International Europhysics Conference on High Energy Physics*, Uppsala, 1987, Ed. Olga Botner.

[14] L. Hall and M. Suzuki, Nucl. Phys. **B231** (1984) 419; V. Barger, G. F. Giudice and T. Han, Phys. Rev. **D40** (1989) 2987; H. Dreiner, hep-ph/9707435.

[15] A. Jodidio *et al.*, Phys. Rev. **D34** (1986) 1967; Phys. Rev. **D37** (1988) 237 erratum.

[16] R. Gill *et al.*, TRIUMF experiment #614 (1993).

[17] J. Prieels *et al.*, PSI experiment R-97-06 (1997).

[18] K. Bodek *et al.*, in *Proc. Symmetries 2000 Conference*, Adelaide, Australia, March 2000.

[19] I.C. Barnett *et al.*, Nucl. Instrum. Meth. **A455** (2000) 329.

[20] S.T. Petcov, Sov. J. Nucl. Phys. **25** (1977) 340; S.M. Bilenky, S.T. Petcov and B. Pontecorvo, Phys. Lett. **B67** (1977) 309; T.P. Cheng and L.-F. Li in *Proceedings of the Coral Gables Conference*, 1977, Ed. Saul Perlmutter (Plenum, New York, 1977).

[21] W. Marciano and A. Sanda, Phys. Lett. **B67** (1977) 303; B.W. Lee, S. Pakvasa, R. Shrock and H. Sugawara, Phys. Rev. Lett. **38** (1977) 937; B.W. Lee and R. Shrock, Phys. Rev. **D16** (1977) 1444.

[22] J. Bernabeu, E. Nardi and D. Tommasini, Nucl. Phys. **B409** (1993) 69.

[23] S. Davidson, D. Bailey and B. Campbell, Z. Phys. **C61** (1994) 613.

[24] S. Coleman and S.L. Glashow, Phys. Rev. **D59** (1999) 116008.

[25] R. Bluhm, V.A. Kostelecky and C.D. Lane, Phys. Rev. Lett. **84** (2000) 1098; H.G. Dehmelt *et al.*, Phys. Rev. Lett. **83** (1999) 4694; V.W. Hughes *et al.*, hep-ex/0106103, to appear in Phys. Rev. Lett.

[26] Y. Kuno and Y. Okada, Rev. Mod. Phys. **73** (2001) 151.

[27] A. Czarnecki, W. J. Marciano and K. Melnikov, in *Proc. Workshop on Physics at the First Muon Collider and at the Front End of the Muon Collider*, Eds. S.H. Geer and R. Raja (AIP Conference Proc. 435), p. 409 [hep-ph/9801218].

[28] M. Raidal and A. Santamaria, Phys. Lett. **B421** (1998) 250.

[29] A. de Gouvêa, S. Lola and K. Tobe, Phys. Rev. **D63** (2001) 035004.

[30] S.B. Treiman, F. Wilczek and A. Zee, Phys. Rev. **D16** (1977) 152.

[31] Y. Okada, K. Okumura and Y. Shimizu, Phys. Rev. **D58** (1998) 051901; **D61** (2000) 094001.

[32] J. Ellis, J. Hisano, S. Lola and M. Raidal, hep-ph/0109125.

[33] H.P. Nilles, Phys. Rep. **110** (1984) 110, and references therein.

[34] J. Hisano *et al.*, Phys. Rev. **D53** (1996) 2442.

[35] M. Dine and A.E. Nelson, Phys. Rev. **D48** (1993) 1277. For a review see G.F. Giudice and R. Rattazzi, Phys. Rep. **322** (1999) 419; **322** (1999) 501.

[36] L.J. Hall, V.A. Kostelecky and S. Raby, Nucl. Phys. **B267** (1986) 415.

[37] F. Borzumati and A. Masiero, Phys. Rev. Lett. **57** (1986) 961; J. Hisano *et al.*, Phys. Lett. **B357** (1995) 579.

[38] J. Hisano, D. Nomura and T. Yanagida, Phys. Lett. **B437** (1998) 351; J. Hisano and D. Nomura, Phys. Rev. **D59** (1999) 116005; M.E. Gomez *et al.*, Phys. Rev. **D59** (1999) 116009; W. Buchmüller, D. Delphine and F. Vissani, Phys. Lett. **B459** (1999) 171; W. Buchmüller, D. Delphine and L.T. Handoko, Nucl. Phys. **B576** (2000) 445; J. Ellis *et al.*, Eur. Phys. J. **C14** (2000) 319; J.L. Feng, Y. Nir and Y. Shadmi, Phys. Rev. **D61** (2000) 113005; S. Baek *et al.*, Phys. Rev. **D63** (2001) 051701; J. Sato, K. Tobe and T. Yanagida, Phys. Lett. **B498** (2001) 189; J. Sato and K. Tobe, Phys. Rev. **D63** (2001) 116010; J. L. Feng, hep-ph/0101122; J. A. Casas and A. Ibarra, hep-ph/0103065; S. Davidson and A. Ibarra, hep-ph/0104076; S. Baek *et al.*, hep-ph/0104146; S. Lavignac, I. Masina and C. A. Savoy, hep-ph/0106245.

[39] J. Ellis *et al.*, Eur. Phys. J. **C14** (2000) 319.

[40] T. Yanagida, in *Proceedings of the Workshop on Unified Theory and Baryon Number of the Universe*, Tsukuba, Japan, 1979, O. Sawada and A. Sugamoto (KEK, Tsukuba, 1979), p. 95; M. Gell-Mann, P. Ramond and R. Slansky, in *Supergravity, Proceedings of the Workshop*, Stony Brook, New York, 1979, Eds. P. van Nieuwenhuizen and D. Freedman (North-Holland, Amsterdam, 1979).

[41] See 'Neutrino Oscillation Physics', this report.

[42] H.N. Brown *et al.*, Phys. Rev. Lett. **86** (2001) 2227.

[43] A number of speculative papers has appeared since the publication of reference [42]. A compilation can be found at `http://phyppro1.phy.bnl.gov/g2muon/new_theory.html`.

[44] J. Hisano and K. Tobe, Phys. Lett. **B510** (2001) 197.

[45] D. F. Carvalho *et al.*, hep-ph/0103256.

[46] M. Graesser and S. Thomas, hep-ph/0104254; Z. Chacko and G. D. Kribs, hep-ph/0104317; T. Ibrahim and P. Nath, hep-ph/0105025.

[47] R. Barbieri and L.J. Hall, Phys. Lett. **B228** (1994) 212.

[48] R. Barbieri, L.J. Hall and A. Strumia, Nucl. Phys. **B445** (1995) 219.

[49] J. Hisano *et al.*, Phys. Lett. **B391** (1997) 341, erratum **B397** (1997) 357.

[50] J. Hisano *et al.*, Phys. Rev. **D58** (1998) 116010.

[51] Y. Kuno and Y. Okada, Phys. Rev. Lett. **77** (1996) 434.

[52] Y. Kuno, A. Maki and Y. Okada, Phys. Rev. **D55** (1997) 2517.

[53] D. Suematsu, Phys. Lett. **B416** (1998) 108; S.F. King and M. Oliveira, Phys. Rev. **D60** (1999) 035003; G. Couture *et al.*, Eur. Phys. J. **C7** (1999) 135; K. Kurosawa and N. Maekawa, Prog. Theor. Phys. **102** (1999) 121; R. Kitano and K. Yamamoto, Phys. Rev. **D62** (2000) 073007; G. Barenboim, K. Huitu and M. Raidal, Phys. Rev. **D63** (2001) 055006.

[54] N. Arkani-Hamed, H.-C. Cheng and L.J. Hall, Phys. Rev. **D53** (1996) 413; P. Ciafaloni, A. Romanino and A. Strumia, Nucl. Phys. **B458** (1996) 3; T.V. Duong, B. Dutta and E. Keith, Phys. Lett. **B378** (1996) 128; N.G. Deshpande, B. Dutta and E. Keith, Phys. Rev. **D54** (1996) 730.

[55] N. Arkani-Hamed, S. Dimopoulos and G. Dvali, Phys. Lett. **B429** (1998) 263.

[56] L. Randall and R. Sundrum, Phys. Rev. Lett. **83** (1999) 3370.

[57] N. Arkani-Hamed *et al.*, preprint hep-ph/9811448; K.R. Dienes, E. Dudas and T. Gherghetta, Nucl. Phys. **B557** (1999) 25; Y. Grossman and M. Neubert, Phys. Lett. **B474** (2000) 361.

[58] A.E. Faraggi and M. Pospelov, Phys. Lett. **B458** (1999) 237; A. Ioannisian and A. Pilaftsis, Phys. Rev. **D62** (2000) 066001; R. Kitano, Phys. Lett. **B481** (2000) 39; T.P. Cheng and L. Li, Phys. Lett. **B502** (2001) 152.

[59] A. de Gouvêa, G.F. Giudice, A. Strumia and K. Tobe, hep-ph/0107156.

[60] See for instance A. E. Pifer *et al.*, Nucl. Instrum. Meth. **135** (1976) 39.

[61] A. van der Schaaf *et al.*, Nucl. Phys. **A340** (1980) 249; H.P. Povel *et al.*, Phys. Lett. **B72** (1977) 183.

[62] P. Depommier *et al.*, Phys. Rev. Lett. **39** (1977) 1113.

[63] W.W. Kinnison *et al.*, Phys. Rev. **D25** (1982) 2846; J.D. Bowman *et al.*, Phys. Rev. Lett. **42** (1979) 556.

[64] R.D. Bolton *et al.*, Phys. Rev. **D38** (1988) 2077; R.D. Bolton *et al.*, Phys. Rev. Lett. **56** (1986) 2461.

[65] M.L. Brooks *et al.*(MEGA Collaboration), Phys. Rev. Lett. **83** (1999) 1521.

[66] L. Barkov *et al.*, Search for $\mu^+ \to e^+ + \gamma$ down to 10^{-14} branching ratio, available at `http://www.icepp.s.u-tokyo.ac.jp/meg`.

[67] S. Korenchenko *et al.*, Search for the decay $\mu^+ \to e^+ + \gamma$ with a branching-ratio sensitivity of 10^{-14}, Letter of Intent for an experiment at PSI, R-98-05.0 (1998).

[68] Y. Kuno, A. Maki and Y. Okada, MEG TN-01/1997.

[69] SINDRUM Collaboration, U. Bellgardt *et al.*, Nucl. Phys. **B299** (1988) 1.

[70] SINDRUM Collaboration, W. Bertl *et al.*, Nucl. Phys. **B260** (1985) 1.

[71] S. Weinberg and G. Feinberg, Phys. Rev. Lett. **3** (1953) 111, 244 (Erratum).

[72] T.S. Kosmas and J.D. Vergados, Phys. Lett. **B217** (1989) 19.

[73] T.S. Kosmas and J.D. Vergados, Nucl. Phys. **A510** (1990) 641.

[74] H.C. Chiang, E. Oset, T.S. Kosmas, A. Faessler and J.D. Vergados, Nucl. Phys. **A559** (1993) 526.

[75] T.S. Kosmas, A. Faessler, F. Šimkovic and J. D. Vergados, Phys. Rev. **C56** (1997) 526.

[76] O. Shanker, Phys. Rev. **D20** (1979) 1608.

[77] F. Herzog and K. Alder, Helv. Phys. Acta **53** (1980) 53.

[78] SINDRUM Collaboration: PSI proposal R-87-09 (1987).

[79] MECO Collaboration: BNL proposal AGS P940 (1997).

[80] SINDRUM II Collaboration, W. Honecker *et al.*, Phys. Rev. Lett. **76** (1996) 200.

[81] B. Pontecorvo, Zh. Eksp. Teor. Fiz. **33** (1957) 549, [Sov. Phys. JETP **6** (1958) 429]; G. Feinberg and S. Weinberg, Phys. Rev. **123** (1961) 1439.

[82] V.W. Hughes *et al.*, Phys. Rev. Lett. **5** (1960) 63; V.W. Hughes and G. zu Putlitz, in: *Quantum Electrodynamics*, Ed. T. Kinoshita (World Scientific, Singapore, (1990) p. 822).

[83] P. Herczeg and R.N. Mohapatra, Phys. Rev. Lett. **69** (1992) 2475; A. Halprin, Phys. Rev. Lett. **48** (1982) 1313; R.N. Mohapatra, Z. Phys. **C56** (1992) 117; G.G. Wong and W.S. Hou, Phys. Rev. **D50** (1994) R2962; A. Halprin and A. Masiero, Phys. Rev. **D48** (1993) 2987; H. Fujii, Y. Mimura, K. Sasaki and T. Sasaki, Phys. Rev. **D49** (1994) 559; P.H. Frampton and M. Harada, Phys. Rev. **D58** (1998) 095013; V. Pleitez, Phys. Rev. **D61** (2000) 057903.

[84] G.G. Wong and W.S. Hou, Phys. Lett. **B357** (1995) 145.

[85] K. Horikawa and K. Sasaki, Phys. Rev. **D53** (1996) 560.

[86] D.L. Morgan Jr. and V.W. Hughes, Phys. Rev. **D2** (1970) 1389; D.L. Morgan Jr. and V.W. Hughes, Phys. Rev. **A7** (1973) 1811.

[87] L. Willmann *et al.*, Phys. Rev. Lett. **82** (1999) 49; L. Willmann and K. Jungmann, Lecture Notes in Physics, Vol. 499 (1997) and references therein.

[88] K. Jungmann, in: *Symmetries in Subatomic Physics*, Eds. X.-H. Guo, A.W. Thomas and A.G. Williams, p. 341 (2000).

[89] M. Davier and A. Höcker, Phys. Lett. **B435** (1998) 427.

[90] F.J.M. Farley and E. Picasso, in: *Quantum Electrodynamics*, E. T. Kinoshita (World Scientific, Singapore, 1990), p. 479; V.W. Hughes and T. Kinoshita, in: *Muon Physics I*, Eds. V. W. Hughes and C.S. Wu (Academic Press, New York, 2000) pp. 12-199.

[91] F.J. Yndurain, hep-ph/0102312.

[92] S. Narison, hep-ph/0103199.

[93] W. Marciano and B.L. Roberts, hep-ph/0105056.

[94] Y.K. Semertzidis, in: *Frontier Tests of Quantum Electrodynamics and Physics of the Vacuum*, Eds. E. Zavattini, D. Baklanov and C. Rizzo (1998) p. 369; R. Carey *et al.*, Letter of Intent to BNL (2000).

[95] K.S. Babu, B. Dutta and R. Mohapatra, hep-ph/0006329 (2000).

[96] I.B. Khriplovich, Phys. Lett. **B444** (1998) 98.

[97] *Proceedings of the Workshop on Nuclear Electric Dipole Moments (NEDM)*, GSI print, Eds. I.B. Khriplovich, J. Kluge, K. Jungmann (1999).

[98] K. Jungmann, Hyperf. Interact. **127** (2000) 189.

[99] P. Mohr and B. Taylor, Rev. Mod. Phys. **72** (2000) 351.

[100] W. Liu *et al.*, Phys. Rev. Lett. **82** (1999) 711.

[101] K. Jungmann, in: *The Hydrogen Atom*, Eds. S. Karshenboim *et al.*, (Springer, Heidelberg, 2001) p. 81 and references therein.

[102] V. Meyer *et al.*, Phys. Rev. Lett. **84** (2000) 1136.

[103] J. Dilling *et al.*, Hyperf. Interact. **127** (2000) 491.

[104] G.L. Borchert *et al.*, Acta Phys. Pol. **B29** (1998) 131.

[105] M.D. Hasinoff, in: *Muonic Atoms and Molecules*, Eds. L. Schaller and C. Petitjean, Birkhäuser, Basel, (1993), p. 13; P.C. Bergbusch, Phys. Rev. **C59** (1999) 2853.

[106] S.G. Karshenboim, Phys. Lett. **A225** (1997) 97; K. Pachucki, Phys. Rev. **A60** (1999) 3593; K. Jungmann, V.G. Ivanov, S.G. Karshenboim, in: Hydrogen Atom II, Springer, in print (2001).

[107] R. Pohl *et al.*, Hyperf. Interact. **127** (2000) 161.

[108] D. Bacalov, E. Milotti, C. Rizzo, A. Vacchi and E. Zavattini, Phys. Lett. **A172** (1993) 277.

[109] *Muon Science*, Eds. S.L. Lee, S.H. Kilcyone and R. Cywinski (Inst. Phys. Publ. Bristol, 1999).

[110] K. Nagamine, in: *Muon Science*, Eds. S.L. Lee, S.H. Kilcyone and R. Cywinski (Inst. Phys. Publ. Bristol, 1999), pp. 313–341.

[111] K. Träger *et al.*, Physica **B289** (2000) 662.

[112] E. Morenzoni, in *Muon Science*, Eds. S.L. Lee, S.H. Kilcyone and R. Cywinski (Inst. Phys. Publ. Bristol, 1999), pp. 343–404.

[113] G.H. Eaton and S.H. Kilcoyne, in *Muon Science*, Eds. S.L. Lee, S.H. Kilcyone and R. Cywinski (Inst. Phys. Publ. Bristol, 1999), pp. 11–37; R. Abela, F. Foroughi and D. Renker, Z. Phys. **C56** (1992) S240; A.E. Pifer *et al.*, Nucl. Instrum. Meth. **135** (1976) 39.

[114] B. Autin *et al.*, *The CERN Neutrino Factory Working Group; Status Report and Work Plan*, Neutrino Factory note 28 (2000), available from `http://muonstoragerings.cern.ch`.

[115] *Conceptual design of the SPL, A High Power Superconducting H- Linac at CERN*, A. Lombardi and M. Vretenar eds, CERN Report in preparation, available from `http://vretenar.home.cern.ch/vretenar/spl-sg/report.html`.

[116] A. Blondel, J.P. Fabre, S. Gilardoni, N. Vassilopoulos, *A Thin Target Scheme for the Muon Source*, Neutrino Factory note 6 (1999), available from `http://muonstoragerings.cern.ch`.

[117] G. Heidenreich, `http://www1.psi.ch/users/HEIDEN/target_facilities.html`.

[118] See for instance the study by J.R.J. Benett (RAL): `http://muonstoragerings.web.cern.ch/muonstoragerings/Events/19990920/Benett.pdf`.